Many-electron effects in multiphoton ionization: Screening effects in single-electron ionization

Anne L'Huillier
Service de Physique des Atomes et des Surfaces, Centre d'Etudes Nucléaires de Saclay, F-91191 Gif-sur-Yvette Cédex, France

Lars Jönsson and Göran Wendin
Institute of Theoretical Physics, Chalmers University of Technology, S-412 96 Göteborg, Sweden
(Received 19 August 1985; revised manuscript received 21 January 1986)

We study the influence of many-electron effects in multiphoton ionization within the framework of diagrammatic many-body perturbation theory. We renormalize the electron-dipole coupling by summing to infinite order both many-electron interactions using the random-phase approximation and higher-order intensity terms. We introduce an effective intensity, which takes into account the screening of the field by the electrons and represents the intensity really seen by an electron. The theory is applied to a calculation of the two-photon one-electron ionization rate of helium in the weak-field limit, using a local-density approximation one-electron basis set. The influence of many-electron effects strongly depends on the field frequency. The two-photon ionization rate of helium is lowered at low frequency (by a factor up to 1.4) and increased at high frequency when the photon energy is above the ionization threshold. Finally, the importance of many-electron effects in multiphoton ionization (e.g., regarding inner-shell ionization) is qualitatively discussed in connection with experiments.

I. INTRODUCTION

Multiphoton ionization of one-electron atoms in weak laser fields (e.g., $< 10^9$ W cm^{-2}) is now a well-known subject, both experimentally and theoretically, and has been extensively reviewed.[1-3] The new challenge brought to theoreticians by recent experiments performed on rare gases can be summarized by the following question: what is the response of a many-electron atom (with several electrons in the outermost shell) to a strong electromagnetic field (10^{12}–10^{16} W cm^{-2})?

This problem has been raised by experimental results obtained in photoelectron energy analysis[4-6] and ion-detection measurements.[7-11] These two experimental techniques yield different but complementary information on the atomic processes. Both types of results have shown that an atom irradiated by an intense laser field can absorb many more photons than the minimum number of photons (N) required for ionization. This leads to the generation of energetic electrons and the production of multiply charged ions.

A photoelectron spectrum obtained in single-electron multiphoton ionization consists of a series of peaks evenly spaced in photon energy corresponding to an N-, $(N+1)$-, ..., $(N+S)$-photon absorption process. For example, in the case of xenon irradiated by a neodymium–yttrium-aluminum-garnet (Nd-YAG) laser (1064 nm) at 10^{13} W cm^{-2}, electrons whose kinetic energy corresponds to an absorption of 11 additional photons in the continuum have been reported.[5] According to perturbation theory, below the onset of saturation (which means depletion of neutral atoms in the interaction region) these peaks should have decreasing amplitudes and vary with the intensity as $I^N, I^{N+1}, \ldots, I^{N+S}$. Some experimental results[5] are at variance with these predictions and theoretical one-electron models[12-16] have been recently proposed for describing these strong-field effects and qualitatively explaining the experiments.

Ion-detection experiments have shown that multiply charged ions can be created through multiphoton absorption: up to Xe^{5+} with a Nd-YAG laser[7,8] (1064 nm, 10^{13} W cm^{-2}), even up to Xe^{8+} with an ArF laser[9-11] (193 nm, 10^{14} W cm^{-2}). Doubly charged helium ions have also been detected at 1064 nm,[8] in a percentage ratio of $\frac{1}{1000}$ at 6×10^{14} W cm^{-2}. This ratio is extremely high considering the difference between the minimum number of photons that have to be absorbed for single (22) and double (68) ionization. Very recently, up to Xe^{3+} ions have been produced with a CO_2 laser[17] (10 μm, 10^{13}–10^{14} W cm^{-2}), which suggests[17] that the tunneling mechanism of Keldysh[18] could be relevant in this case.

Experimental results have emphasized the following points: (i) an enormous energy is transferred to the atom through multiphoton absorption (250 eV to yield Xe^{5+} with photons of typically 1, 2, or 6 eV energy); (ii) doubly charged ions can be created either by a "direct" process from the ground state of neutral atoms or by a "stepwise" process via the singly charged ion in its ground state or an excited state;[7] (iii) lastly, these multiple ionization processes strongly depend on the atomic structure and outermost shell density.[9-11] This suggests that many-electron (collective) effects[19,20] could play an important role in multiphoton ionization of heavy atoms. Several (statistical) models have been developed to account for the distribution of multiply charged ions at very high laser intensity.[21-23]

Many-electron effects in atomic systems submitted to weak external perturbations (linear response) are now fairly well understood.[24–31] Some work has been done in connection with nonlinear optical properties[32] and multiphoton ionization,[33–36] but the understanding is still quite limited. However, this may eventually change because the theory of many-electron effects in multiphoton ionization is presently attracting much attention.[37–45]

In this paper, we outline a theoretical description of the interaction of a many-electron atom with an intense laser field. The formalism which takes into account both the interaction with the field and the Coulomb interaction is nonperturbative in the sense that the interaction (electromagnetic or Coulomb) is allowed to modify the electronic structure. This is accomplished within the framework of diagrammatic perturbation theory by performing partial infinite summations. In this way, the electron-photon and electron-electron interactions and the electron and hole propagators are dressed. As a result, the interactions become screened and the electron and hole levels shifted and broadened.

Section II is devoted to a qualitative picture of the response of a many-electron atom to a time-dependent electromagnetic field. Section III presents the theoretical formalism derived from diagrammatic techniques for single-electron ionization. This is applied to a calculation of the two-photon single-ionization probability of helium in Sec. IV. Lastly, in Sec. V, we attempt to make some contact with experiment and with other theoretical approaches, and we present some views on linear response, nonlinear effects, and multielectron resonances.

II. QUALITATIVE PICTURE OF IONIZATION BY STRONG TIME-DEPENDENT FIELDS

Figure 1 gives a schematic picture of the response of an atom to a time-dependent external field. As long as the frequency ω of the external field is low compared with typical excitation energies of the outermost atomic shell (e.g., the lowest excitation energy, the ionization energy, or a collective frequency), the field will be screened out from the interior of the atom. In the weak-field limit, the frequency ω has to be raised above the first ionization threshold in order to give rise to ionization. This represents ordinary single-photon ionization, excited for instance with synchrotron radiation.

If the outermost shell contains several electrons, the induced fields due to the perturbed electronic density will screen the external field, so that one may think of the electron as being emitted by an effective field at frequency ω (incorporating the many-electron response). The screening will effectively displace the oscillator-strength distribution towards higher energies, in a manner that depends on the polarizability of the atomic shell.[24,25,29,30,46] Often, one has reason to talk in terms of collective effects, as for instance in the case of the $5p^6$ and $4d^{10}$ shells in Xe or Ba,[24] or the $6p$ and $5d$ shells in Th and U.[25]

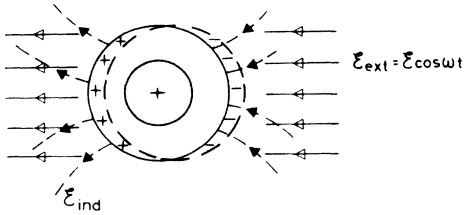

FIG. 1. Schematic picture of the excitation of an atomic system by a time-dependent field.

At high-photon frequencies, finally, the outer atomic shell cannot respond, and the field can penetrate into the inner-shell region. There, however, the procedure repeats itself; the inner shell is stiffer, and will follow the external field until the frequency is further increased to well above the typical excitation or ionization energy of the inner shell. Moreover, at lower frequencies the inner shell will enhance the field in the outer-shell region, leading to increased ionization from the outer shell. These are the typical conditions that govern weak-field, single-photon ionization when the photon energy is varied.[24–31]

Let us now return to low frequencies ω below the first excitation energy of the outermost shell. Increasing the strength of the field will merely increase the magnitude of the response; the external field will still be kept from the interior of the atom, unless it becomes so strong that nonlinear effects and/or tunneling ionization become important. At high laser intensities, multiphoton processes become highly probable, and total field-to-atom energy transfers exceeding the ionization energies of inner shells can be achieved. However, direct multiphoton ionization of the inner shells cannot take place since the component of the field at frequency ω is screened out in the core region. Inner-shell ionization would have to proceed via indirect processes, which only become effective at very high field strengths, e.g., (i) nonlinear processes leading to up conversion and to strong harmonics at frequencies high enough not to be screened by the outer shell; (ii) generation of fast photoelectrons from the outer shell, leading to impact ionization of the inner shell;[19] (iii) stripping of the outer shell (which screens the core) during the first part of the pulse followed by ionization of the remaining core in a later part of the pulse.[47]

III. MULTIPHOTON SINGLE-ELECTRON IONIZATION WITHIN A MANY-ELECTRON FORMULATION

In the following, we shall imagine that the final-state electron(s) can be measured using photoelectron spectroscopy. A schematic picture of a photoelectron spectrum is shown in Fig. 2. Observation of a particular photoelectron (PE) line with kinetic energy $\varepsilon=\varepsilon_i+N\omega$ determines the number of photons being absorbed. In addition, an arbitrary number of photons may be absorbed and reemitted. The amplitude $t_\varepsilon(\omega;N;I)$ [Fig. 2(b)] takes into account intensity (I) effects, as well as correlation effects like polarization and relaxation in a many-electron system. The resulting photoelectron spectrum (current) is given by

$$\mathcal{I}_\varepsilon(\omega;N;I)\propto |t_\varepsilon(\omega;N;I)|^2\delta(\varepsilon-\varepsilon_i-N\omega)\ . \tag{3.1}$$

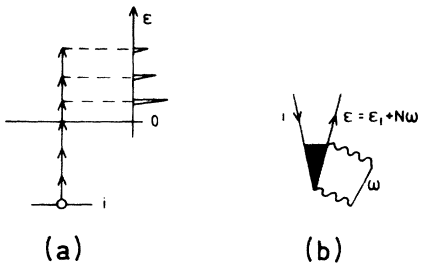

FIG. 2. General representation of N-photon single-electron ionization. (a) Energy scheme; (b) diagrammatic picture, intensity (space between two wavy lines) and correlation (solid triangle) effects are systematically included.

The amplitude $t_\varepsilon(\omega;N;I)$ can be broken down into various more or less elementary processes. To begin with, we shall consider an effective one-electron problem and, in particular, the influence of the field on the photoelectron.

A. One-electron formulation

A diagrammatic formulation of the N-photon one-electron ionization amplitude is shown in Fig. 3(a). The wavy box represents absorption of N photons plus absorption and reemission of an arbitrary number of photons. The exact summation of higher-order intensity terms in

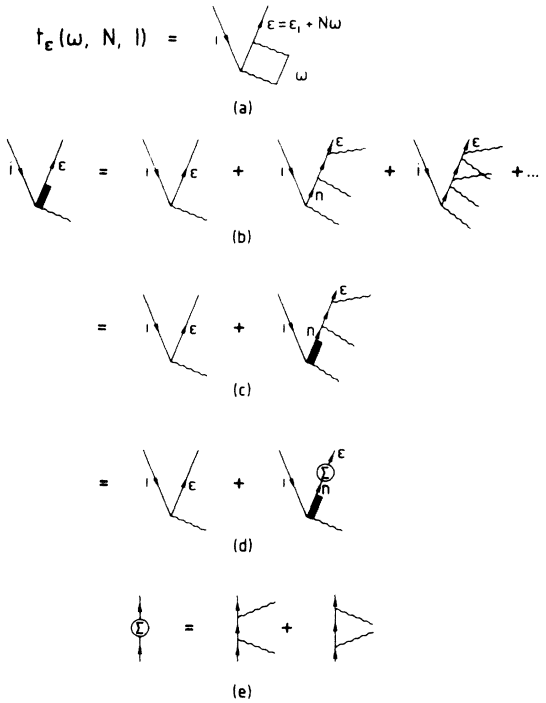

FIG. 3. One-electron formulation. (a) Diagrammatic representation of the N-photon ionization amplitude; the space between two wavy lines represents a N-photon absorption plus any higher-order process of photon absorption and emission. (b)—(d) Diagrammatic representation of the effective dipole matrix element $D^1_{\varepsilon i}$ including repeated photon absorption and reemission process, (b) perturbation expansion, (c) integral equation, (d) in terms of a Stark-shift self-energy defined in (e). (e) Stark-shift self-energy.

the perturbation expansion is a major problem. We do not pretend to offer any general solutions, but we think that a few important aspects can be discussed in a fairly simple way.

We shall first consider one-photon absorption, $N=1$, as shown in Fig. 3(b). The excitation of a bound electron (i) to the continuum (ε,n), followed by the repeated one-photon absorption and reemission, may be represented by an effective one-photon ionization dipole matrix element $D^1_{\varepsilon i}(\omega)$, given by the perturbation series [Fig. 3(b)]

$$D^1_{\varepsilon i}(\omega)=d_{\varepsilon i}+I\sum_{m,n}\frac{d_{\varepsilon m}d_{mn}d_{ni}}{(\omega_{mi}-2\omega)(\omega_{ni}-\omega)}$$
$$+I^2\times(\cdots)+\cdots\,, \tag{3.2}$$

or by the corresponding integral equation [Fig. 3(c)]

$$D^1_{\varepsilon i}(\omega)=d_{\varepsilon i}+I\sum_{m,n}\frac{d_{\varepsilon m}d_{mn}}{(\omega_{mi}-2\omega)(\omega_{ni}-\omega)}D^1_{ni}(\omega)\,. \tag{3.3}$$

Equations (3.2) and (3.3) are obtained by applying usual diagrammatic evaluation rules (see, e.g., Refs. 48—50) to the diagrams represented in Figs. 3(b) and 3(c). We are using a basis of one-electron states, typically Hartree-Fock; ε_m and ε_i denote one-electron energy eigenvalues and $\omega_{mi}=\varepsilon_m-\varepsilon_i$ represent one-electron excitation energies. The electron-photon coupling is given by

$$\langle m\,|\,\mathbf{E}\cdot\mathbf{r}\,|\,n\rangle=I^{1/2}\langle m\,|\,\hat{\mathbf{e}}\cdot\mathbf{r}\,|\,n\rangle \tag{3.4a}$$
$$=I^{1/2}d_{mn}\,. \tag{3.4b}$$

We shall adopt the following notations for the electron-photon coupling: the lower-case letters (d,d^N) represent the ordinary one-photon or N-photon matrix elements; the upper-case letters $[D^1(\omega),D^N(\omega)]$ represent the "Stark-shifted" matrix elements (renormalized in the field interaction); $[d(\omega),d^N(\omega)]$ denote the matrix elements screened at frequency ω (many-electron polarization effects are included); lastly, the script letters $[\mathscr{D}^1(\omega,p\omega),\mathscr{D}^N(\omega)]$ represent the complete matrix elements renormalized both in electron-photon and electron-electron interaction.

Equation (3.3) may be written in terms of a Stark-shift self-energy $\Sigma(\omega)$ [Fig. 3(d)],

$$D^1_{\varepsilon i}(\omega)=d_{\varepsilon i}+\sum_n\frac{\Sigma_{\varepsilon n}(\omega)}{\omega_{ni}-\omega}D^1_{ni}(\omega)\,, \tag{3.5}$$

and we may also extend $\Sigma(\omega)$ to including processes where the order of one-photon absorption and reemission are interchanged,

$$\Sigma_{\varepsilon n}(\omega)=I\sum_m\left[\frac{d_{\varepsilon m}d_{mn}}{\omega_{mi}-2\omega}+\frac{d_{\varepsilon m}d_{mn}}{\omega_{mi}}\right]. \tag{3.6}$$

An approximate (nonperturbative) solution of the integral equation (3.5) for the effective one-photon matrix element $D^1_{\varepsilon i}(\omega)$ is given by

$$D^1_{\varepsilon i}(\omega)=d_{\varepsilon i}+\sum_n\frac{\Sigma_{\varepsilon n}(\omega)d_{ni}}{\omega_{ni}-\omega}\Big/F(\omega) \tag{3.7}$$

with

$$F(\omega)=1-\sum_n \frac{\Sigma_{nn}(\omega)}{\omega_{ni}-\omega} . \tag{3.8}$$

The solution in Eq. (3.7) is of the Fredholm type and has the great advantage that it is correct to first order in $\Sigma(\omega)$: the approximate result (3.7) retains the correct structure of Eq. (3.5), and the factorization only enters when turning the higher-order corrections into a geometric series. A much more approximate form, which would be valid if the interaction were factorizable (which it is not), is given by

$$D^1_{\varepsilon i}(\omega)=d_{\varepsilon i}/F(\omega) . \tag{3.9}$$

The zeros of $F(\omega)$ in Eq. (3.8) give the poles of the Stark-shifted excitation spectrum. In the neighborhood of a discrete excitation n, Eq. (3.7) becomes

$$D^1_{\varepsilon i}(\omega)=d_{\varepsilon i}+\frac{\Sigma_{\varepsilon n}(\omega)d_{ni}}{\omega_{ni}-\Sigma_{nn}(\omega)-\omega} , \tag{3.10}$$

which describes a Stark-shifted intermediate resonance. In the continuum, $F(\omega)$ will lead to a change in the continuum density of states.

The above description merely represents a systematic, and probably well-known, treatment of weak-field one-photon ionization. The Stark-shift self-energy $\Sigma(\omega)$ in Eq. (3.6) is only calculated to first order in the intensity I, and systematically going to higher order represents a major problem. The infinite-order problem has been extensively studied for a one-electron system[51–53] but not for any many-electron system. In this paper, however, we shall only consider the Stark shift to first order in the intensity of the photon field.

In order to generalize in a simple way to N-photon ionization, we shall assume that circularly polarized light is used to step only upwards in angular momentum in absorption, $l\rightarrow l+1$, and downwards in emission, $l\rightarrow l-1$. The unperturbed N-photon one-electron matrix element [Fig. 4(a), no Stark shifts] has the form

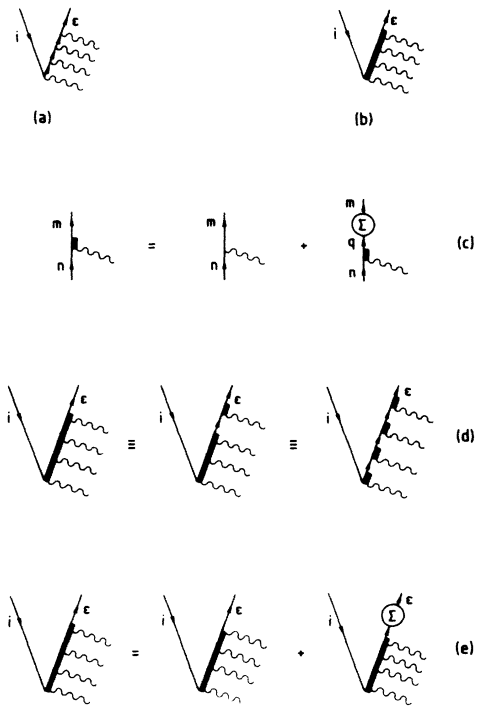

FIG. 4. One-electron formulation. Diagrammatic representation of the N-photon ionization matrix element (a) $d^N_{\varepsilon i}$, (b) $D^N_{\varepsilon i}(\omega)$, (c) intensity-renormalized electron-photon coupling $D^1_{mn}(p\omega)$, (d) different ways of partitioning $D^N_{\varepsilon i}(\omega)$ [Eq. (3.12)], (e) integral equation [Eq. (3.15)].

$$d^N_{\varepsilon i}=\sum_n \frac{d_{\varepsilon n}d^{N-1}_{ni}}{\omega_{ni}-(N-1)\omega} , \tag{3.11a}$$

$$d^N_{\varepsilon i}=\sum_{m_1,m_2,\ldots,m_{N-1}} \frac{d_{\varepsilon m_{N-1}}\cdots d_{m_2m_1}d_{m_1i}}{[\omega_{m_{N-1}i}-(N-1)\omega]\cdots(\omega_{m_2i}-2\omega)(\omega_{m_1i}-\omega)} . \tag{3.11b}$$

We now wish to represent the effect of the Stark-shift self-energy in terms of an effective one-electron dipole matrix element $D^1_{mn}(p\omega)$ leading from $(n,(p-1)\omega)$ to $(m,p\omega)$ [Fig. 4(c)]. The effective N-photon matrix element is defined as

$$D^N_{\varepsilon i}(\omega)=\sum_n \frac{D^1_{\varepsilon n}(N\omega)D^{N-1}_{ni}(\omega)}{\omega_{ni}-(N-1)\omega} , \tag{3.12a}$$

$$D^N_{\varepsilon i}(\omega)=\sum_{m_1,m_2,\ldots,m_{N-1}} \frac{D_{\varepsilon m_{N-1}}(N\omega)\cdots D_{m_2m_1}(2\omega)D_{m_1i}(\omega)}{[\omega_{m_{N-1}i}-(N-1)\omega]\cdots(\omega_{m_2i}-2\omega)(\omega_{m_1i}-\omega)} , \tag{3.12b}$$

where [Fig. 4(c)] ($p=1,2,\ldots,N$)

$$D^1_{mn}(p\omega)=d_{mn}+\sum_q \frac{\Sigma_{mq}(p\omega)}{\omega_{qi}-p\omega}D^1_{qn}(p\omega) , \tag{3.13}$$

and where $\Sigma_{mq}(p\omega)$ is given to lowest order as in (3.6) (Ref. 54),

$$\Sigma_{mq}(p\omega)=I\sum_n \left[\frac{d_{mn}d_{nq}}{\omega_{ni}-(p+1)\omega}+\frac{d_{mn}d_{nq}}{\omega_{ni}-(p-1)\omega}\right] . \tag{3.14}$$

In order to have an integral equation for the N-photon amplitude $D_{\varepsilon i}^{N}(\omega)$, we multiply Eq. (3.13) from the right by $D_{ni}^{N-1}(\omega)$ and sum over n (we also let $m\rightarrow\varepsilon$ and $p\rightarrow N$). As a result

$$D_{\varepsilon i}^{N}(\omega)=D_{\varepsilon i}^{N}+\sum_{n}\frac{\Sigma_{\varepsilon n}(N\omega)}{\omega_{ni}-N\omega}D_{ni}^{N}(\omega)\ , \tag{3.15}$$

where

$$D_{\varepsilon i}^{N}=\sum_{n}\frac{d_{\varepsilon n}D_{ni}^{N-1}(\omega)}{\omega_{ni}-(N-1)\omega}\ . \tag{3.16}$$

Equations (3.11)–(3.13) and (3.15) have been graphically interpreted in Fig. 4. Equation (3.11b) is represented by Fig. 4(a) and the intensity-renormalized Eq. (3.12b) by Fig. 4(b). The integral equation (3.13) for the intensity-renormalized electron coupling is described by Fig. 4(c). Figure 4(d) illustrates the different ways of partitioning the full N-photon matrix element $D_{\varepsilon i}^{N}(\omega)$ in Eq. (3.12), while Fig. 4(e) graphically describes the integral equation (3.15).

Using the Fredholm approximation, the effective one-electron matrix element $D_{mn}^{1}(p\omega)$ [Eq. (3.13)] is given by

$$D_{mn}^{1}(p\omega)\simeq d_{mn}+\sum_{q}\frac{\Sigma_{mq}(p\omega)d_{qn}}{w_{qi}-p\omega}\Big/F(p\omega) \tag{3.17a}$$

$$\simeq d_{mn}/F(p\omega)\ , \tag{3.17b}$$

where

$$F(p\omega)=1-\sum_{n}\frac{\Sigma_{nn}(p\omega)}{\omega_{ni}-p\omega} \tag{3.18a}$$

$$=1-I\beta_{0}(p\omega)\ , \tag{3.18b}$$

with

$$\beta_{0}(p\omega)=\sum_{n,q}\frac{|d_{nq}|^{2}}{\omega_{ni}-p\omega}\left[\frac{1}{\omega_{qi}-(p+1)\omega}+\frac{1}{\omega_{qi}-(p-1)\omega}\right]\ . \tag{3.19}$$

$\beta_{0}(p\omega)$ is related to the Stark shift and represents an inverse characteristic intensity. In the neighborhood of resonances, $\beta_{0}(p\omega)$ shows large and rapid variations with energy, and the zeros of $F(p\omega)$ give the Stark-shifted resonances. However, even when $\beta_{0}(p\omega)$ varies slowly, $F(p\omega)$ may become zero if the intensity is sufficiently large. This would correspond to new levels induced by the field.

It is very instructive to evaluate Eq. (3.12b) using the approximative dipole matrix elements in Eq. (3.17b). The result for the Stark-shift-corrected effective N-photon one-electron matrix element then becomes

$$D_{\varepsilon i}^{N}(\omega)\simeq\frac{d_{\varepsilon i}^{N}}{F(N\omega)\cdots F(2\omega)F(\omega)}\ , \tag{3.20}$$

where $d_{\varepsilon i}^{N}$ is given by Eq. (3.11) (no intensity renormalization).

The photoelectron current can now be written approximately as

$$\mathcal{I}_{\varepsilon}(\omega;N;I)\propto\left[\prod_{p=1}^{N}\frac{I}{[1-I\beta_{0}(p\omega)]^{2}}\right]\times|d_{\varepsilon i}^{N}|^{2}\delta(\varepsilon-\varepsilon_{i}-N\omega)\ . \tag{3.21}$$

At low intensity, the current shows the usual I^{N} power dependence given by perturbation theory. At higher intensities, the renormalization factors may change this power dependence. At very high powers [$I\beta_{0}(p\omega)\gg1$], an entirely different intensity dependence can appear, but then the present low-intensity expansion of the Stark shift may no longer be valid.

It should be emphasized that nonlinear effects have not been included in the formulation leading to Eq. (3.12) in the sense that no components of the field are oscillating at other frequencies than the fundamental frequency ω. We shall only consider nonlinear effects in connection with a system of *interacting* electrons. The electron-electron interaction can be mediated either by photons [at $\omega,3\omega,5\omega,\ldots$, i.e., only odd harmonics; see Figs. 5(a)–5(c)] or by the Coulomb interaction [at $\omega,2\omega,3\omega,\ldots$, i.e., *all* harmonics; see Figs. 5(d)–5(g)]. Figure 5(a) could involve a spontaneous emission at ω. Note that the spontaneous processes indicated in Figs. 5(a)–5(c) should be extremely weak (negligible). Figures 5(d)–5(g) describe various harmonic components of the *induced* field and will be discussed in the following section.

B. Many-electron formulation

The next step in our treatment must be to investigate how the many-electron interaction effects can be included in the one-electron picture given above. A complete many-electron formulation would contain all aspects of polarization, relaxation, and correlation including a whole host of additional nonlinear effects. The many-electron

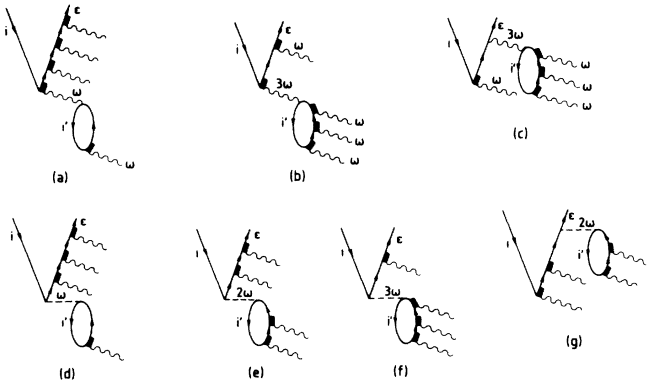

FIG. 5 Examples of linear and nonlinear effects which have not been included in the one-electron formulation (see text).

problem is a formidable problem already in the case of one-photon weak-field ionization, and we have no intention to provide any general discussion in this paper. Instead, we shall concentrate on many-electron polarization effects which screen the external time-dependent radiation field and consequently modify the electron-photon coupling.

A nice aspect is that some important effects of polarization can be included in the same way as the Stark-shift interaction Σ, as shown in Fig. 6 . However. the structure of the integral equation describing the N-photon matrix element $\mathscr{D}^N(\omega)$ is not as simple as (3.15) due to ground-state correlation effects (last diagram in Fig. 6) which introduce negative frequency denominators. As long as we neglect these effects and restrict ourselves to the forward-propagating diagrams (the first three diagrams to the right of the equality in Fig. 6), the combined problem is still described by an integral equation analogous to (3.15), in which the Coulomb interaction is added to the Stark-shift self-energy $\Sigma(N\omega)$,

$$\mathscr{D}^N_{\varepsilon i}(\omega)=\mathscr{D}^N_{\varepsilon i}+\sum_n \frac{[\Sigma_{\varepsilon n}(N\omega)+V_{i\varepsilon ni}]}{\omega_{ni}-N\omega}\mathscr{D}^N_{ni}(\omega)\ . \tag{3.22}$$

As might be expected, there is then no clear distinction between effects of the field and effects of the Coulomb interaction. In particular, at high intensities, effects of the field may win over the electron-electron interaction.

In spite of the advantages of a unified picture, it can be more convenient to separate out the many-electron effects, in order explicitly to obtain screened (renormalized) electron-photon and electron-electron interactions which describe the zero-intensity limit. Figure 7(a) shows diagrammatically the random-phase approximation (RPA) (Refs. 24 and 27) for the electron-photon dipole interaction. (Note that the screened interaction could alternatively be represented by an open circle in the following.) We shall assume, for sake of simplicity, that exchange effects [i.e., electron-hole ladders, RPAE (random-phase-approximation exchange)] are included in the one-electron description. The random-phase approximation (RPAE) describes many-electron polarization effects, and is in particular capable of handling collective effects.[24,46] The screened electron-photon interaction can also be constructed with the screened electron-hole interaction as shown in Figs. 7(b) and 7(c). The RPA integral equation for the dipole matrix element screened at frequency ω, $d_{mn}(\omega)$ [from Fig. 7(a)], can be written as

$$d_{mn}(\omega)=d_{mn}-\sum_{q,j}\frac{2\omega_{qj}V_{mjnq}}{\omega^2_{qj}-\omega^2}d_{qj}(\omega)\ , \tag{3.23}$$

where V_{mjnq} is the Coulomb matrix element

$$V_{mjnq}=\langle mj\,|\,|\mathbf{r}-\mathbf{r}'|^{-1}\,|\,nq\rangle\ . \tag{3.24}$$

If the polarizability of the outermost atomic shell is large, the field strength inside the atom may greatly differ from the field strength outside. Obviously, this should be of particular importance in nonlinear processes, because it will lead to a renormalization of the coupling constant. In analogy with Eq. (3.4), we may write the electron-photon coupling as

$$\begin{aligned} I^{1/2}d_{mn}&\rightarrow I^{1/2}d_{mn}(\omega)\\ &=I^{1/2}\langle m\,|\,\hat{\mathbf{e}}\cdot\mathbf{r}(\omega)\,|\,n\rangle\ , \end{aligned} \tag{3.25}$$

where

$$\hat{\mathbf{e}}\cdot\mathbf{r}(\omega)=\hat{\mathbf{e}}\cdot\mathbf{r}-\sum_{q,j}\frac{2\omega_{qj}\langle j\,|\,|\mathbf{r}-\mathbf{r}'|^{-1}\,|\,q\rangle d_{qj}(\omega)}{\omega^2_{qj}-\omega^2}\ . \tag{3.26}$$

$\langle j\,|\,|\mathbf{r}-\mathbf{r}'|^{-1}\,|\,q\rangle$ involves an integration over $\mathbf{r}'$ (the one-electron states refer to $\mathbf{r}'$). Equation (3.26) corresponds exactly to Fig. 7(a).

The screened dipole operator $\mathbf{r}(\omega)$ may be rewritten in terms of a space-dependent inverse dielectric function (response function) $\epsilon^{-1}(\mathbf{r},\omega)$ as (see also Refs. 24, 29, 30, and 55)

$$\hat{\mathbf{e}}\cdot\mathbf{r}(\omega)=\epsilon^{-1}(\mathbf{r},\omega)\hat{\mathbf{e}}\cdot\mathbf{r}\ . \tag{3.27}$$

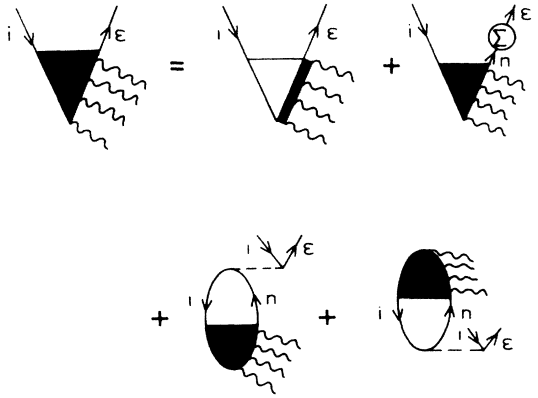

FIG. 6. Many-electron formulation (1). Diagrammatic representation of the effective N-photon matrix element $\mathscr{D}^N_{\varepsilon i}(\omega)$; the first diagram to the right of the equality is $D^N_{\varepsilon i}$ defined as in (3.14), the next one includes the interaction with the field, and the last two diagrams the Coulomb interaction.

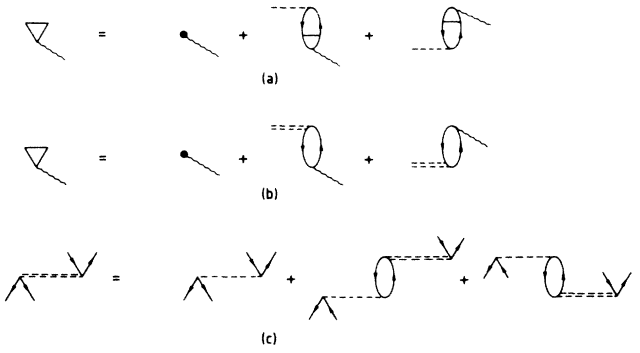

FIG. 7. Random-phase approximation. (a) Integral equal for the screened electron-photon interaction, (b) screened electron-photon interaction constructed with (c), (c) screened electron-hole interaction.

The effective electron-photon interaction may now be expressed in a number of ways:

$$I^{1/2}d_{mn}(\omega)=\langle m\mid\epsilon^{-1}(\mathbf{r},\omega)\mathbf{E}\cdot\mathbf{r}\mid n\rangle \tag{3.28a}$$

$$=\langle m\mid\mathbf{E}_{\rm eff}(\mathbf{r},\omega)\cdot\mathbf{r}\mid n\rangle \tag{3.28b}$$

$$=\langle\mathbf{E}_{\rm eff}(\omega)\rangle_{mn}\langle m\mid\hat{\mathbf{e}}\cdot\mathbf{r}\mid n\rangle \tag{3.28c}$$

$$=I^{1/2}\langle\epsilon^{-1}(\omega)\rangle d_{mn} \tag{3.28d}$$

$$=\langle I^{1/2}_{\rm eff}(\omega)\rangle d_{mn}\ . \tag{3.28e}$$

The coupling depends on the local effective dielectric field [Eq. (3.28b)]. Furthermore, we may define a state-dependent average electric field [Eq. (3.28c)] or dielectric function (3.28d) or intensity (3.28e). In Eqs. (3.28d) and (3.28e) we have omitted explicit mention of the state dependence, but it should be understood: the average $\langle\ \rangle$ effectively refers to a limited region of space which gives the main contribution to the matrix element.

We can now return to the combined problem of the nonperturbative description of both the field and Coulomb interaction. We first screen Coulomb and dipole matrix elements as in Fig. 7 and replace the ordinary matrix elements by the screened ones in order systematically to include the many-electron linear response at frequency ω. The Stark-shift self-energy in Eq. (3.14) will then explicitly depend on ω as well as on $p\omega$, $\Sigma(p\omega)\rightarrow\Sigma(\omega,p\omega)$.

The presence of negative frequencies in the RPA expansion (we do not restrict ourselves to forward-propagating diagrams but include ground-state correlations) requires that the generalization of (3.5) is a matrix equation, involving an effective Stark-shift self-energy matrix $\Sigma^{\mu\nu}(\omega,p\omega)$ ($p=1,2,\ldots N$, $\mu,\nu=\pm$), defined in Fig. 8(a). In the case of one-photon absorption ($N=1$), the two components $(\mathscr{D}^{1+},\mathscr{D}^{1-})$ of the total electron-photon dipole operator are solutions of the following coupled equations [Fig. 8(b)]:

$$\mathscr{D}^{1+}_{\varepsilon i}(\omega)=d_{\varepsilon i}+\sum_n\left[\frac{\Sigma^{++}_{\varepsilon n}(\omega)}{\omega_{ni}-\omega}\mathscr{D}^{1+}_{ni}(\omega)+\frac{\Sigma^{-+}_{\varepsilon n}(\omega)}{\omega_{ni}+\omega}\mathscr{D}^{1-}_{ni}(\omega)\right], \tag{3.29a}$$

$$\mathscr{D}^{1-}_{\varepsilon i}(\omega)=d_{\varepsilon i}+\sum_n\left[\frac{\Sigma^{--}_{\varepsilon n}(\omega)}{\omega_{ni}+w}\mathscr{D}^{1-}_{ni}(\omega)+\frac{\Sigma^{+-}_{\varepsilon n}(\omega)}{\omega_{ni}-\omega}\mathscr{D}^{1+}_{ni}(\omega)\right]. \tag{3.29b}$$

For N-photon absorption ($N>1$) equations similar to (3.29) may be derived for the effective one-photon one-electron dipole matrix $\mathscr{D}^{1\pm}(\omega,p\omega)$ ($p=2,3,\ldots,N$). A systematic treatment can fairly easily be expressed in diagrammatic form, but the corresponding analytical expressions will be very bulky. The aim of the present paper is, however, to demonstrate the role of many-electron screening in the low-intensity limit (Stark shifts $\sim I$), not to present any complete treatment. We shall therefore introduce a number of simplifications, some of which might have to be reconsidered in connection with numerical calculations or for reasons of consistency (sum rules, etc.).

To begin with, we only keep forward-propagating diagrams for $\Sigma^{\mu\nu}(\omega,p\omega)$, leaving only $\Sigma^{++}(\omega,p\omega)$. Equation (3.29) may then be generalized to the p-photon level [Fig. 8(c)] ($\mathscr{D}^{1+}\equiv\mathscr{D}^{1}$ from now on):

$$\mathscr{D}^{1}_{mn}(\omega,p\omega)=d_{mn}(\omega,p\omega)+\sum_q\frac{\Sigma^{++}_{mq}(\omega,p\omega)}{\omega_{qi}-p\omega}\mathscr{D}^{1}_{qn}(\omega,p\omega)\ , \tag{3.30}$$

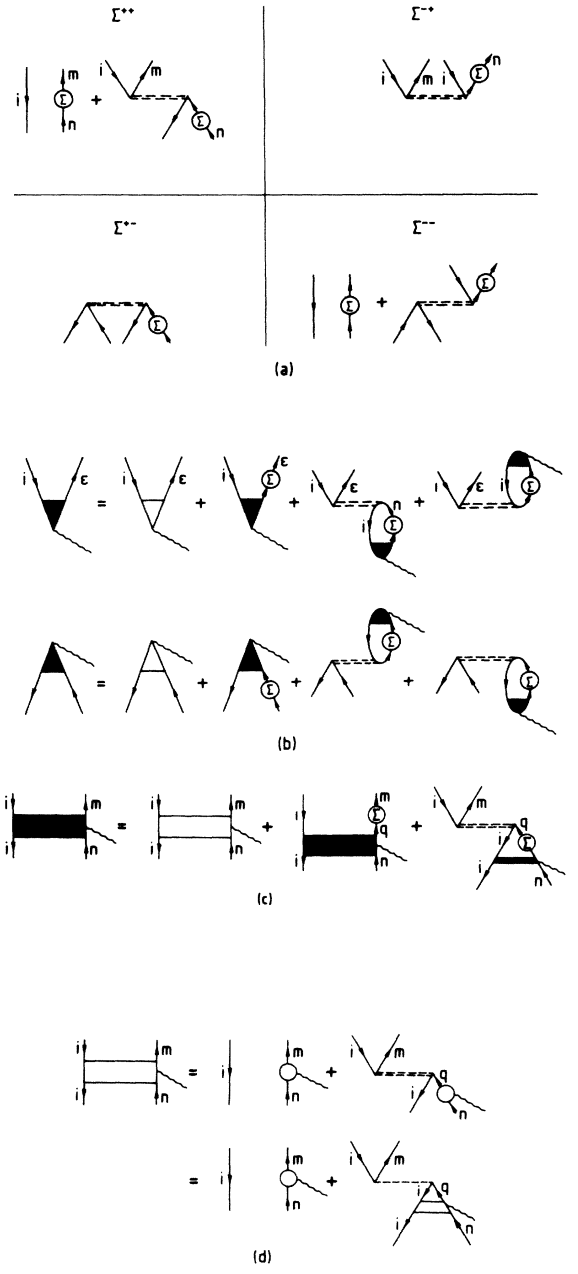

FIG. 8. Many-electron formulation (2). (a) Stark-shift self-energy matrix, (b) matrix equation for the one-photon matrix element $\mathscr{D}^{1\pm}_{\varepsilon i}(\omega,\omega)$ screened at frequency ω and Stark shifted, (c) one-photon matrix element $\mathscr{D}^{1\pm}_{mn}(\omega,p\omega)$ screened at ω and $p\omega$ and Stark shifted, (d) one-photon matrix element $d_{mn}(\omega,p\omega)$ screened at ω and $p\omega$ and not Stark shifted.

where [Fig. 8(d)]

$$d_{mn}(\omega,p\omega)=d_{mn}(\omega)-\sum_q \frac{2\omega_{qi}V_{miiq}(p\omega)}{\omega_{qi}^2-(p\omega)^2}d_{qn}(\omega)\ , \tag{3.31}$$

and where [Fig. 8(a)]

$$\Sigma_{mq}^{++}(\omega,p\omega)=\Sigma_{mq}(\omega,p\omega)-\sum_n \frac{V_{miin}(p\omega)\Sigma_{nq}(\omega,p\omega)}{\omega_{ni}-p\omega}\ . \tag{3.32}$$

The Stark-shift self-energy $\Sigma_{mq}(\omega,p\omega)$ depends on the screened dipole matrix elements

$$\Sigma_{mq}(\omega,p\omega)=I\sum_n\left[\frac{d_{mn}(\omega)d_{nq}(\omega,(p+1)\omega)}{\omega_{ni}-(p+1)\omega}+\frac{d_{mn}(\omega)d_{nq}(\omega,(p-1)\omega)}{\omega_{ni}-(p-1)\omega}\right]\ . \tag{3.33}$$

$V_{miiq}(p\omega)$ is a matrix element of the Coulomb interaction [Fig. 7(c)] screened at frequency $p\omega$ [given by an integral equation similar to Eq. (3.23) with $\omega\rightarrow p\omega$]. $d_{mn}(\omega,p\omega)$ [Eq. (3.31), Fig. 8(d)] can also be written as the solution of an integral equation

$$d_{mn}(\omega,p\omega)=d_{mn}(\omega)-\sum_q \frac{2\omega_{qi}V_{miiq}}{\omega_{qi}^2-(p\omega)^2}d_{qn}(\omega,p\omega)\ . \tag{3.34}$$

Equation (3.34) says that *the screened electric field has frequency components at* $p\omega$, so that the pth photon will be screened both at frequency ω and $p\omega$. This is really an example of *nonlinear effects;* the induced electric field will have components at $\omega,2\omega,3\omega,\ldots$ (Fig. 5).

$\mathscr{D}_{mn}^1(\omega,p\omega)$ in Eq. (3.30) is the fundamental quantity in the N-photon ionization matrix element [cf. Eq. (3.12)]

$$\mathscr{D}_{\varepsilon i}^N(\omega)=\sum_{m_1,m_2,\ldots,m_{N-1}}\frac{\mathscr{D}_{\varepsilon m_{N-1}}(\omega,N\omega)\cdots\mathscr{D}_{m_2m_1}(\omega,2\omega)\mathscr{D}_{m_1i}(\omega,\omega)}{[\omega_{m_{N-1}i}-(N-1)\omega]\cdots(\omega_{m_2i}-2\omega)(\omega_{m_1i}-\omega)}\ . \tag{3.35}$$

Note that Eq. (3.35) only represents a direct generalization of Eq. (3.12) to include screening of the one-photon dipole matrix elements, $D^1(p\omega)\rightarrow\mathscr{D}^1(\omega,p\omega)$. A completely general expression would also contain all the nonlinear combinations [e.g., Fig. 5(g)].

The approximate effects of the screening can easily be extracted by introducing some further simplifications. The purpose is to find approximate expressions for the dipole matrix elements in Eq. (3.35). First, we use the Fredholm approach[56,57] to obtain approximate solutions of the integral equations. We introduce the definitions

$$F(\omega,p\omega)=1-\sum_n\frac{\Sigma_{nn}^{++}(\omega,p\omega)}{\omega_{ni}-p\omega}\ , \tag{3.36}$$

$$\epsilon_+(p\omega)=1+\sum_n\frac{V_{niin}}{\omega_{ni}-p\omega}\ , \tag{3.37}$$

$$\epsilon(p\omega)=1+\sum_n\frac{2\omega_{ni}V_{niin}}{\omega_{ni}^2-(p\omega)^2}\ . \tag{3.38}$$

Equation (3.30) then becomes

$$\mathscr{D}_{mn}^1(\omega,p\omega)\simeq d_{mn}(\omega,p\omega)/F(\omega,p\omega)\ . \tag{3.39}$$

Using Eq. (3.34), we further obtain

$$\mathscr{D}_{mn}^1(\omega,p\omega)\simeq\begin{cases}d_{mn}(\omega)/F(\omega,\omega) & (p=1) \quad (3.40)\\ d_{mn}(\omega)/\epsilon(p\omega)F(\omega,p\omega) & (p>1)\ . \quad (3.41)\end{cases}$$

The difference between Eqs. (3.40) and (3.41) arises because for $p>1$ there are two independent screening mechanisms (independent in the present treatment) at ω and $p\omega$.

In a similar way, Eq. (3.32) approximately becomes

$$\Sigma_{nn}^{++}(\omega,p\omega)\simeq\Sigma_{nn}(\omega,p\omega)/\epsilon_+(p\omega)\ . \tag{3.42}$$

In the present approximation, the intensity dependence of the dipole matrix elements only enters through $F(\omega,p\omega)$. To lowest order in the intensity I, Eq. (3.42) becomes

$$\Sigma_{nn}^{++}(\omega,p\omega)\simeq I\epsilon_+^{-1}(p\omega)\sum_q|d_{nq}(\omega)|^2\times\left[\frac{\epsilon^{-1}((p+1)\omega)}{\omega_{qi}-(p+1)\omega}+\frac{\epsilon^{-1}((p-1)\omega)}{\omega_{qi}-(p-1)\omega}\right], \tag{3.43}$$

so that $F(\omega,p\omega)$ in Eq. (3.36) may be written as

$$F(\omega,p\omega)=1-I\,|\langle\epsilon^{-1}(\omega)\rangle\epsilon^{-1}(p\omega)|^2\beta(p\omega) \tag{3.44a}$$

$$=1-\langle I_{\rm eff}(\omega)\rangle\,|\epsilon^{-1}(p\omega)|^2\beta(p\omega) \tag{3.44b}$$

$$=1-\langle I_{\rm eff}(\omega,p\omega)\rangle\beta(p\omega)\ , \tag{3.44c}$$

where

$$\beta(p\omega)=\frac{\epsilon(p\omega)}{\epsilon_+(p\omega)}\times\sum_{n,q}\frac{|d_{nq}|^2}{\omega_{ni}-p\omega}\left[\frac{\epsilon(p\omega)\epsilon^{-1}((p+1)\omega)}{\omega_{qi}-(p+1)\omega}+\frac{\epsilon(p\omega)\epsilon^{-1}((p-1)\omega)}{\omega_{qi}-(p-1)\omega}\right]. \tag{3.45}$$

$\beta(p\omega)$ is similar to the one-electron Stark-shift quantity $\beta_0(p\omega)$ in Eq. (3.19), but with modifications due to the dielectric functions. However, firstly, we suspect that a more complete (systematic) treatment will replace $\epsilon_+(p\omega)$ by $\epsilon(p\omega)$ in Eq. (3.45) (and elsewhere). Secondly, as long as $\epsilon(p\omega)$ varies slowly with energy, then $\epsilon(p\omega)\simeq\epsilon((p+1)\omega)\simeq\epsilon((p-1)\omega)$. Equation (3.45) will therefore

effectively reduce to the Stark-shift expression $\beta_0(p\omega)$ describing noninteracting electrons.

The N-photon ionization current (3.1) from the ith subshell has the explicit form

$$\mathcal{I}_\varepsilon(\omega;N;I)\propto I^N\,|\,\mathcal{D}^N_{\varepsilon i}(\omega)\,|^2\delta(\varepsilon-\varepsilon_i-N\omega)\,, \tag{3.46}$$

where $\mathcal{D}^N_{\varepsilon i}(\omega)$ is given by Eq. (3.30). A sum over the electrons in the ith subshell is understood. With the approximate expressions (3.40) and (3.41) for the one-photon dipole matrix elements, we finally obtain

$$\mathcal{I}_\varepsilon(\omega;N;I)=S(\omega;N)\mathcal{I}_{0\varepsilon}(\omega;N;I)\,, \tag{3.47}$$

where

$$\mathcal{I}_{0\varepsilon}(\omega;N;I)\propto I^N\,|\,d^N_{\varepsilon i}\,|^2\delta(\varepsilon-\varepsilon_i-N\omega)\,, \tag{3.48}$$

$$S(\omega;N)=\left|\frac{\langle\epsilon^{-1}(\omega)\rangle^N\epsilon^{-1}(N\omega)\cdots\epsilon^{-1}(2\omega)}{F(\omega,N\omega)\cdots F(\omega,2\omega)F(\omega,\omega)}\right|^2. \tag{3.49}$$

$\mathcal{I}_{0\varepsilon}(\omega;N;I)$ is the current obtained from lowest-order perturbation theory for the electron-dipole coupling, while $S(\omega;N)$ describes higher- (infinite) order dynamic effects due to dressing of the electrons by the field and due to many-electron screening.

The average dielectric function in Eq. (3.49) should be interpreted according to

$$\langle\epsilon^{-1}(\omega)\rangle^N=\langle\epsilon^{-1}(\omega)\rangle_N\cdots\langle\epsilon^{-1}(\omega)\rangle_2\langle\epsilon^{-1}(\omega)\rangle_1\,, \tag{3.50}$$

meaning that the screening is state dependent and may be different for each dipole matrix element.

Equations (3.47)—(3.49) may also be written in a form analogous to the one-electron equation (3.22),

$$\mathcal{I}_\varepsilon(\omega;N;I)\propto I^N_{\rm eff}\,|\,d^N_{\varepsilon i}\,|^2\delta(\varepsilon-\varepsilon_i-N\omega)\,, \tag{3.51}$$

where

$$I^N_{\rm eff}=\prod_{p=1}^{N}\frac{\langle I_{\rm eff}(\omega,p\omega)\rangle}{|\,1-\langle I_{\rm eff}(\omega,p\omega)\rangle\beta(p\omega)\,|^2}\,, \tag{3.52}$$

with

$$\begin{aligned}\langle I_{\rm eff}(\omega,p\omega)\rangle&=I\,|\,\langle\epsilon^{-1}(\omega)\rangle\epsilon^{-1}(p\omega)\,|^2\\&=I\,|\,\langle\epsilon^{-1}(\omega,p\omega)\rangle\,|^2\quad(p>1)\\\langle I_{\rm eff}(\omega,\omega)\rangle&=I\,|\,\langle\epsilon^{-1}(\omega)\rangle\,|^2\\&=\langle I_{\rm eff}(\omega)\rangle\quad(p=1)\,.\end{aligned} \tag{3.53}$$

The result for interacting electrons in Eqs. (3.51)—(3.53) can therefore be directly obtained from the result for noninteracting independent electrons in Eq. (3.22) essentially by *replacing the external field intensity I by a screened, effective field intensity $\langle I_{eff}(\omega,p\omega)\rangle$*.

Equations (3.47) and (3.51) have been designed to demonstrate the role of screening and renormalization. The idea is, of course, that one might be able to identify a typical average effective field in a region where the N-photon ionization amplitude essentially is formed.

The starting point for proper calculations is Eq. (3.30) combined with Eqs. (3.35) and (3.46). In that case, the screened field will be properly evaluated within the dipole matrix element in a state-dependent manner [Eqs. (3.28a) and (3.28b)] without reference to any average field. However, a better approach would then be first to perform the intermediate sums, going over to a space representation with Green's functions (integration over coordinates is understood),

$$\mathcal{D}^N_{\varepsilon i}(\omega)=\langle\varepsilon\,|\cdots G(\mathbf{r}',\mathbf{r};p\omega)\epsilon^{-1}(\mathbf{r},\omega,p\omega)\hat{\mathbf{e}}\cdot\mathbf{r}G(\mathbf{r},\mathbf{r}'';(p-1)\omega)\cdots\,|\,i\rangle\,, \tag{3.54}$$

as in fact we do in Sec. IV (see also Appendix A). From Eq. (3.53), it is clear that it is the spatial extent of the wave packet $\int d\mathbf{r}''[G(\mathbf{r},\mathbf{r}'';p\omega)\cdots]\,|\,i\rangle$ that determines which part of the screening function (effective field) $\epsilon^{-1}(\mathbf{r},\omega,p\omega)$ is effective.

An equation equivalent to Eq. (3.54) with $\epsilon^{-1}(\mathbf{r},\omega,p\omega)=\epsilon^{-1}(\mathbf{r},\omega)$ (only screening at ω) has been used by Zangwill[32] for calculating third-order nonlinear polarizabilities in the rare gases (third-harmonic generation). We shall also use this simplification and neglect the screening at $p\omega$ ($p=2$) in the numerical applications in the next section.

IV. CALCULATION OF TWO-PHOTON SINGLE IONIZATION OF HELIUM

The theoretical methods presented in Sec. III have been applied to the simplest case, the two-photon single ionization of the helium $1s^2\,{}^1S$ state in the weak-field limit (the interaction with the electromagnetic field is treated perturbatively). The purpose of the calculation is not to obtain any accurate results which would anyway be difficult to compare with experiment due to the very high photon energy required (>12 eV), but to analyze polarization effects on the two-photon absorption process when the photon energy is varied below and above the ionization threshold.

A. One-electron approximation

In the central-field approximation, one-electron wave functions are expanded in spherical harmonics:

$$\psi_{nlm}(r,\theta,\phi)=\frac{1}{r}u_{nl}(r)Y_{ml}(\theta,\phi)\,, \tag{4.1}$$

with u_{nl} being the solution of the radial Schrödinger equation (Ry units)

$$\left[-\frac{d^2}{dr^2}-2\frac{Z}{r}+V(r)+\frac{l(l+1)}{r^2}\right]u_{nl}(r)=\varepsilon_{nl}u_{nl}(r)\,. \tag{4.2}$$

$V(r)$ is the sum of the electrostatic potential V_H (Hartree term) and an exchange/correlation potential V_{xc}. The Hartree-Fock approximation neglects correlations but accounts exactly for exchange effects. Here, we shall use a local-density approximation (LDA) (Refs. 24, 29, 30, and 58) which contains local exchange and some part of the correlations, describing the potential according to

$$V_{xc}(r) \sim -\rho^{1/3} . \tag{4.3}$$

Due to the local-density approximation of the exchange potential, there is no longer perfect cancellation between the self-interaction from the direct term and the self-interaction from the exchange term. In other words, an electron at large distances sees a neutral atom (V^N potential). Therefore, the LDA potential does not support any Rydberg levels. In particular, for helium, which is an extreme case, no bound p states exist. As a consequence, the two-photon ionization probability will not show any resonances due to bound excited states. However, very good results have been obtained by using a LDA one-electron basis set to calculate one-photon ionization cross sections.[24,25,29] The LDA potential correctly describes the continuum part of the spectrum; it also gives a good description of the average oscillator-strength distribution in the discrete region. For example, the dynamic polarizability is well described at low frequencies and above the ionization threshold.

Although the local-density approximation has been applied to many atoms, it has never been used, as far as we know, to calculate the one-photon ionization cross section for helium. In order to check its validity for helium, we have performed an RPA calculation with the LDA basis set and calculated the photoionization cross section.

B. One-photon ionization cross section

The one-photon ionization cross section may be written

$$\sigma(\omega) = 4\pi^2 \alpha a_0^2 \omega \, | \, d_{\varepsilon p\, 1s}(\omega) \, |^2 , \tag{4.4}$$

where α is the fine-structure constant, a_0 the Bohr radius, ω the field frequency, and $d_{\varepsilon p\, 1s}(\omega)$ the screened dipole matrix element for the transition $1s \rightarrow \varepsilon p$ [Eqs. (3.25) and (3.26)]:

$$d_{\varepsilon p\, 1s}(\omega) = \langle \varepsilon p \, | \, \epsilon^{-1}(\mathbf{r},\omega) \hat{\mathbf{e}} \cdot \mathbf{r} \, | \, 1s \rangle . \tag{4.5}$$

The numerical methods used to calculate $\epsilon^{-1}(\mathbf{r},\omega)$ are described in Appendix A.

Figure 9 shows a plot of the photoionization cross section (Mb) as a function of the photon energy (Ry). The numerical result for the cross section (4.4) is represented by the dot-dashed line. The dashed line corresponds to the one-electron approximation [Eq. (4.4) with the usual (not screened) dipole matrix element $d_{\varepsilon p\, 1s}$]. The dotted line is an RPA calculation with a Hartree-Fock (HF) one-electron basis.[59] The solid line is an experimental result.[60] The ionization threshold given by the LDA potential (1.13 Ry) is much lower than the real one (1.81 Ry). The part of the spectrum below 1.81 is an average representation of the photoabsorption spectrum (transitions towards discrete states). From about 3 Ry, the local-density RPA result is in very good agreement with experimental data, and is even closer than the RPA result obtained with a HF basis.

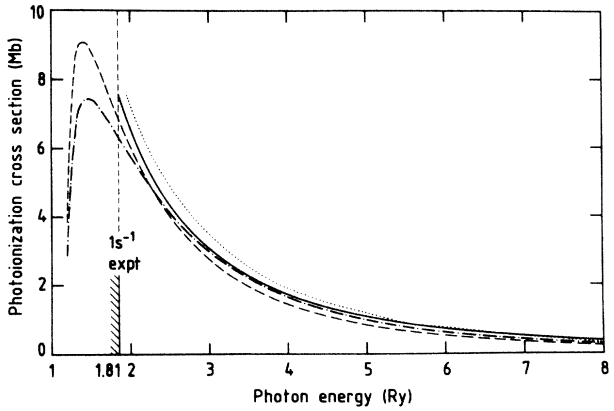

FIG. 9. Photoionization cross section of helium (Mb) as a function of the photon energy in rydbergs; (— — —) one-electron approximation with a LDA basis, (— · — · —) random-phase approximation with a LDA basis, (. . . .) random-phase approximation with a HF basis (Ref. 60) (——) experimental data (Ref. 59).

C. Two-photon ionization probability

The two-photon ionization rate for a linearly polarized light can be written as

$$p = 2\pi(\alpha c/a_0)(I/I_0)^2 [\, | \, d^2_{\varepsilon d\, 1s}(\omega) \, |^2 + | \, d^2_{\varepsilon s\, 1s}(\omega) \, |^2] , \tag{4.6}$$

where c is the light velocity, I_0 a normalization factor equal to 14.038×10^{16} W cm^{-2}, I the laser intensity in W cm^{-2}, $d^2_{\varepsilon l\, 1s}(\omega)$ the renormalized two-photon matrix element ($l = s$ or d). From Eq. (3.54),

$$d^2_{\varepsilon l\, 1s}(\omega) = \langle \varepsilon l \, | \, \epsilon^{-1}(\mathbf{r},\omega,2\omega) \hat{\mathbf{e}} \cdot \mathbf{r} G(\mathbf{r},\mathbf{r}',\omega) \epsilon^{-1}(\mathbf{r}',\omega) \hat{\mathbf{e}} \cdot \mathbf{r}' \, | \, 1s \rangle , \tag{4.7}$$

with

$$G(\mathbf{r},\mathbf{r}',\omega) = \sum_n \frac{| np \rangle \langle np |}{\omega_{np\, 1s} - \omega} . \tag{4.8}$$

As already mentioned in Sec. III, we shall not consider the screening at frequency 2ω: $\epsilon^{-1}(\mathbf{r},\omega,2\omega) \simeq \epsilon^{-1}(\mathbf{r},\omega)$. The diagrams calculated within this approximation are represented in Fig. 10(b). The diagrams related to the screening at 2ω which are represented in Fig. 10(b) involve monopole or quadrupole Coulomb interactions and can be disregarded in a first approximation as will be briefly discussed in Appendix B. The method used to calculate

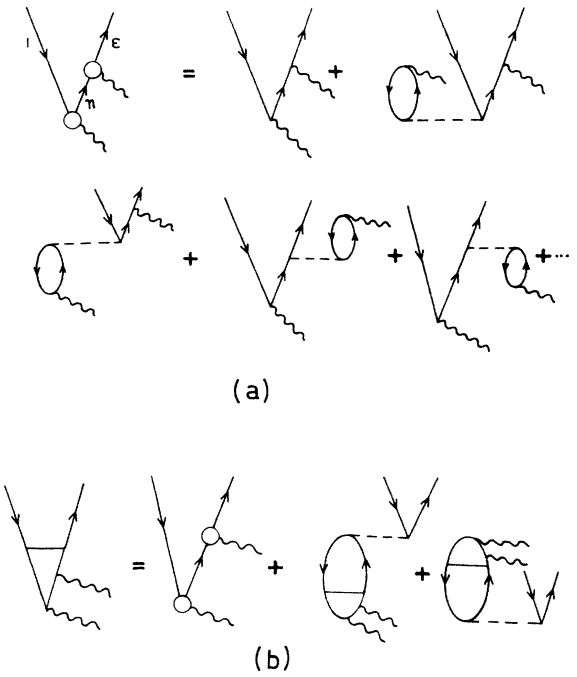

FIG. 10. Diagrammatic representation of the two-photon single-ionization amplitude (a) screened at ω, (b) screened at ω and 2ω.

$\epsilon^{-1}(\mathbf{r},\omega)$ and $G(\mathbf{r},\mathbf{r}',\omega)$ when the photon is varied below and above the ionization energy (involving real and complex Green's functions) are detailed in Appendix A.

Figure 11 shows a plot of the ionization rate divided by the square of the laser intensity, p/I^2, in 10^{-16} $s^{-1}W^{-2}cm^4$ units as a function of the photon energy from 0.6 to 2.5 Ry. The solid line is the RPA calculation and the dashed line corresponds to the one-electron approximation. In Fig. 12, the contributions of the continuum s and d transitions to the total rate have been separat-

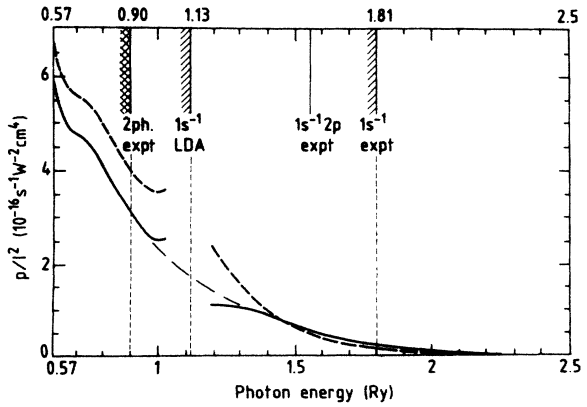

FIG. 11. Plot of the two-photon ionization rate divided by I^2 (in 10^{-16} $s^{-1}W^{-2}cm^4$) as a function of the photon energy (in rydbergs); (— — —) one-electron approximation, (——) random-phase approximation.

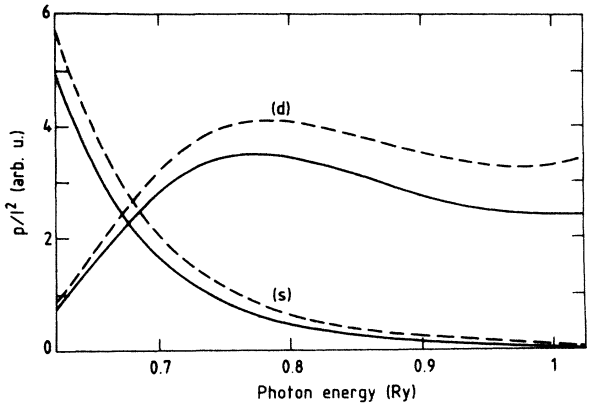

FIG. 12. Contributions of the transitions $1s \rightarrow \varepsilon s$ and $1s \rightarrow \varepsilon d$ to the two-photon ionization process; (— — —) one-electron approximation, (——) random-phase approximation.

ed (the photon energy is varied from 0.6 to 1.0 Ry, i.e., below the ionization threshold). The contribution of the $1s \rightarrow \varepsilon d$ transition is dominant, except at threshold.

The unusual shape of the two-photon ionization rate curve (absence of resonances and very low ionization threshold) is due to the local-density approximation. The LDA ionization threshold is at 1.13 Ry. The two-photon LDA ionization cross section therefore starts at $\omega=0.57$ Ry and shows pronounced structure around $\omega=1.13$ Ry. For computational reasons, we have avoided the close vicinity of the LDA threshold, which explains the gaps in the curves. Moreover, since the experimental ionization threshold is at 1.81 Ry and the two-photon threshold at 0.9 Ry (cf. Fig. 11), the photon-energy range in Fig. 11 may be divided into four regions.

(i) $0.57 < \omega < 0.90$. The photon energy is smaller than the real minimum energy required for a two-photon ionization (0.90 Ry). The spectrum is an average representation of the two-photon absorption spectrum (transitions to discrete levels).

(ii) $0.90 < \omega < 1.13$. The intermediate state of the two-photon transition lies in the discrete part of the spectrum (both real and LDA).

(iii) $1.13 < \omega < 1.81$. The intermediate state is in the discrete part of the real spectrum, but in the continuum of the LDA spectrum. The result can be regarded as an average representation of the two-photon ionization spectrum.

(iv) $\omega > 1.81$. The intermediate state lies in both the real and LDA continua. The local-density approximation is expected to give a good description of this region.

In summary, a realistic approximation to the average two-photon ionization cross section for He starts at $\omega=0.90$ Ry, follows first the solid curve in Fig. 11, then the dash-dotted interpolation (the LDA threshold does not exist in the real spectrum), and finally again the solid curve. The $1s \rightarrow np$ resonances in the 1.40–1.81-Ry region of the real spectrum are thus represented by an average cross section.

An essential result in Fig. 11 is that polarization effects are not negligible at all. Their influence on the two-

photon ionization rate depends on the photon energy. At low energies, the external field is quasistatically screened by polarization effects. For example, at 1 Ry, the two-photon ionization rate is lowered by a factor of 1.4. This effect is reversed around 1.5 Ry. This enhancement of the two-photon ionization rate at large photon energies could be much more important for heavier atoms such as xenon or barium.

D. Comparison with other results

The only calculations that we are aware of for the two-photon ionization probability of ground state He are those of Victor[33] and Ritchie.[34] In Fig. 13, we have plotted our result extrapolated around the LDA threshold (solid line), one result obtained by Victor[33] (solid circles) for $0.95<\omega<1.40$, and one by Ritchie[34] for $0.90<\omega<1.80$ (dashed line). We have taken what we think are the most accurate results obtained by these authors. Victor calculates the two-photon ionization rate of He within the framework of the linearized time-dependent Hartree-Fock (TDHF) approximation.[61] The method used by Ritchie is quite similar; he neglects the negative-frequency terms in the TDHF coupled equations.

The TDHF and RPAE approaches have been shown to be equivalent.[62] The main difference between our result (obtained by considering only the screening at ω, not nonlinear screening, i.e., at frequency 2ω) and those of Victor or, to a lesser extent, Ritchie is then the zeroth-order monoelectronic basis set: LDA in our case, HF in the calculation of Victor or Ritchie. The HF excited spectrum is much closer to the experimental one than the LDA. Consequently, the two-photon ionization rate calculated by Ritchie exhibits resonances on the $1s2p$ and $1s3p$ states. However, away from these resonances, i.e., for $0.90<\omega<1.40$, the results represented in Fig. 13 are in very good agreement. The two-photon LDA spectrum can be viewed as (i) an extension of the HF spectrum to the discrete absorption region ($\omega<0.90$) and above the ionization limit ($\omega>1.81$), (ii) an average of the HF spectrum in the region of the resonances on the $2p$ and $3p$ levels.

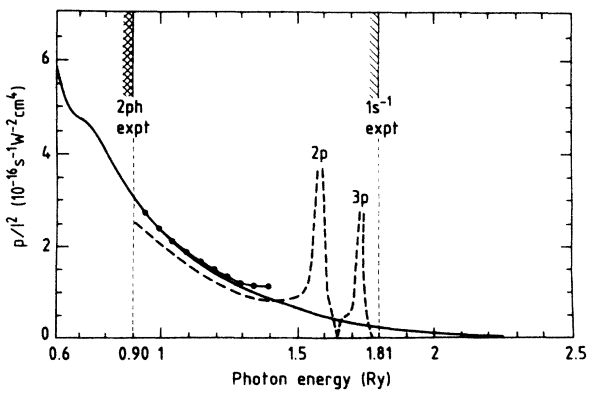

FIG. 13. Comparison between our result (——) (LDRPA) and calculations from Victor (Ref. 35) (•-•-•) and Ritchie (Ref. 34) (— — —) (TDHF).

This comparison proves the validity of the LDA potential for calculating two-photon ionization rates. Moreover, it shows the close similarity between different theoretical approaches, the TDHF theory and the random-phase approximation.

V. DISCUSSION OF THE IMPORTANCE OF MANY-ELECTRON EFFECTS IN MULTIPHOTON IONIZATION

Recent experiments[4–11,17] have raised a number of very interesting questions concerning, for example, (i) absence of inner-shell ionization up to very high intensities, (ii) multiple ionization[7–11,17] up to complete removal of the external shell,[9–11] (iii) deviations from power-law dependence of the photoelectron current at high intensities,[5] (iv) pronounced variation of the average energy transfer with atomic number (Fig. 2 of Ref. 10), and (v) nonlinear effects.

Most of these effects are connected with heavy atoms with many electrons in the region of the outermost shell, like Xe or U. These atoms are well known for their collectivelike properties in single-photon ionization,[24,25] and in core-level spectra.[63] Many-electron effects can therefore be expected to play an important role also in multiphoton ionization of these systems.

The present treatment, leading to the N-photon one-electron ionization current in Eqs. (3.47) and (3.51), addresses the role of many-electron screening within the RPA (linear response). This focuses attention on the total effective field and intensity at frequency ω, and on the effective electron-photon coupling.

One of the major results so far is that the expression for the one-electron current in Eq. (3.51) is valid also with inclusion of many-electron screening provided that the intensity is associated with the effective field [Eq. (3.52)]. In fact, this is a result that one intuitively might expect to find.

As an example, let us study the case of multiphoton ionization of the $5p$ and $4d$ shells in Xe. The physics is illustrated in Fig. 1, and has been qualitatively discussed in Sec. II. The effective field is governed by $\epsilon^{-1}(\mathbf{r},\omega,p\omega)$ $[\simeq\epsilon^{-1}(\mathbf{r},\omega)\epsilon^{-1}(p\omega)]$ as discussed in Eqs. (3.26)–(3.28) and Eq. (3.53). Some previous studies[24,29,30] of the spatial properties of $\epsilon^{-1}(\mathbf{r},\omega)$ as a function of the frequency in the case of the $4d$ shell in Ba have shown that, as long as the frequency lies well below the $4d$ ionization threshold, the dielectric function $\epsilon^{-1}(\mathbf{r},\omega)$ strongly reduces the total field inside the $4d$ shell. This behavior is a general phenomenon and may be applied also to the $5p$ and $6s$ shells of barium as well as to the $5p$ shell of Xe. All the experiments so far have used photon energies (0.1–6 eV) well below the $5p$ ionization energy of xenon ($\sim$12 eV). We may then expect the field to be reduced in the outer-shell $5p$ region and strongly reduced in the inner-shell $4d$ region. We have performed explicit calculations with the local-density random-phase approximation (LDRPA) which show that in the $4d$ region the dielectric function varies from $\langle\epsilon^{-1}(\omega=0)\rangle_{4d}\simeq0.2$ to $\langle\epsilon^{-1}(\omega=6)\rangle_{4d}\simeq-0.2$. In the $5p$ region, the corresponding variation is from $\langle\epsilon^{-1}(\omega=0)\rangle_{5p}\simeq0.7$ to

$\langle \epsilon^{-1}(\omega=6)\rangle_{5p} \simeq 0.5$. In the $4d$ region the effective intensity is therefore reduced by a factor of 25 or more, while in the $5p$ region there is a reduction of the effective intensity at frequency ω by a factor of 2—4. We now discuss in some detail the points (i)—(v) above.

(i) Inner-shell ionization. We conclude that direct multiphoton ionization of the $4d$ shell should largely be prevented through screening by the $5s$ and $5p$ shells. We suggest that this might explain why it is possible to have high-order multielectron ionization of the $5p$ shell, with energy transfers well exceeding the $4d$ ionization energy, and still not observe any $4d$-ionization (e.g., through Auger emission): the effective intensity is strongly reduced in the $4d$ shell region due to the outer-shell screening.

These considerations on the spatial dependence of the effective field may be generalized to any atom with several electrons in the external shell and confirm what has been already qualitatively discussed in Sec. II. Direct inner-shell multiphoton ionization of atoms with a dense outermost shell is a very improbable process because the effective field seen by an inner electron is much weaker than the external field (or the field experienced by an outer electron). We think that the situation is somewhat similar to the case of a metal surface or a metal particle, surface plasmons screening the field and preventing it from penetrating deeply into the metal.

(ii) Multiple ionization. Screening effects also reduce multiphoton ionization in the external shell. Their importance is related to the number of electrons in the external shell. The effective intensity experienced by a Xe $5p$ electron is reduced by a factor of 2—4 ($\omega=0$—6 eV) compared to the experimental intensity. On the other hand, the effective intensity for a Xe^{5+} $5p$ electron or a Xe^{7+} $5s$ electron coincides with the experimental intensity (no screening effect).

We assume that the dominating process for multiple ionization of Xe is stepwise ionization, the electrons being successively removed during the rise of the laser pulse. In this picture, the relative ease with which highly charged ions are removed might partly be understood in terms of reduced screening; as the charge state increases during the stripping, the number of electrons in the external shell will decrease and the screening will be reduced. The effective intensity therefore increases and the ionization becomes more and more easy.

Let us investigate in greater detail the influence of screening in, e.g., the multiple ionization of xenon at 532 nm.[7] The dependence of the number of ions created as a function of the laser intensity is shown in Fig. 3 of Ref. 7. We assume that these ions are created through stepwise processes and that each step occurs in an intensity range for which the preceding steps are saturated. Consequently, the experimental curves represent one-electron multiphoton ionization processes which take place in different atoms (Xe—Xe^{4+}). We now imagine that these curves are drawn as a function of the *effective intensity,* i.e., the intensity that the atomic electrons actually experience. The intensity range over which the ions appear will then be expanded by about a factor of 3 towards *lower* intensities; Xe^{+} will actually appear at about three times lower *local intensity* than suggested by the nominal laser intensity. As a consequence, the screening *reduces the laser (external) intensity range* in which the multiphoton ionization processes are detected.

The introduction of the effective intensity allows us to reduce the problem to a *one-electron* multiphoton ionization problem. One might compare ionization cross sections calculated assuming that the electrons are independent to experimental results provided the intensity is replaced by the effective intensity.

(iii) Photoelectron spectrum. We now present some speculative ideas on the influence of many-electron screening on the photoelectron spectrum obtained in one-electron multiphoton ionization. The screening of the field in the Xe $5p$ region should influence the absolute and relative intensities of the $N, N+1, \ldots, N+S, \ldots$ photoelectron peaks from $5p$ emission [Fig. 2(a)]. One might speculate that in $(N+S)$-photon ionization, the amplitude will sample a region that extends further outside the $5p$ shell for $S>0$ than for $S=0$ and will therefore experience a stronger effective field. This could lead to spectral strength being shifted towards the higher-energy $N+S$ peaks in comparison with a model of noninteracting electrons.

However, the disappearance of the first peaks in the photoelectron spectrum has also been observed in neon and helium[64] for which many-electron screening effects are not very important. Although the role of many-electron screening for creating an effective intensity would deserve a careful investigation in the case of xenon, it certainly does not represent the fundamental mechanism behind the deviations from power-law dependence (see, e.g., Refs. 12—16). That problem is related to intensity renormalization *à la* Eq. (3.52).

(iv) Influence of Z in multiphoton ionization. Finally, we would like to make some suggestions, based on the importance of screening, to interpret the strong variations of the average energy transfer with atomic number, as discussed by Rhodes and co-workers.[9,10]

According to this analysis,[9] Xe and U stand out among the investigated elements with very large energy transfers (65 and 55 eV, respectively). The other rare gases have 2—3 times lower average energy transfers which can possibly (and simply) be understood in terms of their large outer-shell ionization energies. In Xe, two-photon ionization is possible ($\omega \simeq 6.4$ eV), while in Kr, Ar, and Ne, three-photon absorption is necessary for ionization.

Yb presents an extreme at the other end with an average energy transfer about five times lower than for Xe. First of all, $5p$ multiple ionization should be reduced due to screening by the $6s$ shell and due to the large $5p$ ionization energy. Secondly, the $4f$ electrons which have low binding energies are well shielded from the laser field by the $6s$ and $5p$ shells. Consequently, only the $6s^2$ shell and possibly a few $5p$ electrons can easily be removed from Yb. The same should be true for the entire rare-earth sequence [e.g., Eu (Ref. 10) or Ca (Ref. 47)].

In this perspective, the large energy transfer in U looks very interesting. Uranium has the ground-state configuration $5d^{10}5f^{3}6s^{2}6p^{6}6d^{1}7s^{2}$. Arguing as in the case of Yb, we would say that the $5f^3$ electrons should be screened

and essentially nonparticipating. This leaves 11 electrons between the $6s$ and $7s$ shells. The experimental observation of U^{10+} (Ref. 10) then would mean that the $n=6$ and 7 shells essentially have been stripped. However, we also note that if we only consider the shells with the lowest binding energies, there are 10 electrons in the $6p^4{}_{3/2}$, $6d^1$, $5f^3$, and $7s^2$ shells. Moreover, the "valence"-electron distribution $5f^x6d^y7s^z$ is determined by configuration interaction, which may influence the screening arguments above. It seems that Th ($5f^06d^27s^2$) should be an interesting system to compare with.

The low energy transfer of iodine (about four times less than Xe) seems quite anomalous. It might be due to a combination of (interdependent) factors: lower $5p$ binding energy, more efficient $5p$ screening, reduced number of $5p$ electrons, multielectron resonance effects. In general, the large variations in ion spectra and energy transfer point to the necessity of being able to vary the photon energy in order to separate resonance effects from effects of the average electronic structure and dynamics. Detection of photoelectrons should further make it possible to determine which shells are being ionized, like, e.g., whether the $4f$ and $5f$ electrons participate in the ionization of Eu, Yb, and U. Moreover, in this way, one might be able to observe chemical shifts of the orbital energies and draw conclusions about the chemical state of the system (free atoms, molecules, clusters, etc.), which could influence the screening response and the ionization process in important ways.

(v) Nonlinear effects. By considering N-photon ionization of an atomic system, by definition we are studying the nonlinear response of the system, $\sim I^N$. Moreover, by including the dynamic Stark-shift effect, we go beyond a limited power-series expansion in the intensity [Fig. 4, Eq. (3.22)]. Nevertheless, in other respects, we have neglected the nonlinear response, e.g., by omitting diagrams like Fig. 5(a) [note, however, that we have included the nonlinear processes in Figs. 5(e) and 5(f)], and by neglecting higher harmonics of the laser field.

Moreover, in the present treatment, the screened electron-photon interaction in Figs. 7 and 8 has been taken to be independent of the state of the system by ignoring the Coulomb interaction between the electron-hole pairs describing the polarizability and the electron-hole pairs already excited in the system [Fig. 14(a)]. Inclusion of the Coulomb interaction leads to nonadditivity of the electron-hole pair excitation energies and to state dependence of the polarizability. For example, Fig. 14(b) describes a contribution to the screening of three photons where the polarization bubbles do not interact with each other. This diagram has been included through linear screening of each individual electron-photon interaction, and eventually includes resonance frequencies involving only *single-electron* excitations. On the other hand, we have neglected any corrections due to nonadditivity of electron-hole pair excitation energies in multiple electron excitations [Fig. 14(c)]. Multiple-electron excitations provide a mechanism for exciting large-amplitude collective motion of, e.g., the $5p$ shell in Xe (collective "mode" with several quanta) (cf. Refs. 43 and 44). The decay of this multielectron excitation may proceed in a number of ways, e.g., via stepwise energy transfer at the fundamental frequency ω [Fig. 14(c)] or at higher harmonics [Figs. 14(d) and 14(e)].

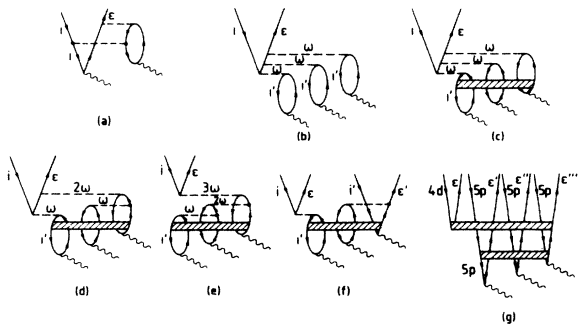

FIG. 14. Effects of the Coulomb interaction in multielectron excitations (see text).

Finally, there is also the very important possibility of *resonant multiple ionization* [Fig. 14(f)]. A multiply excited resonance can autoionize, and for a collective type of resonance one can expect the ionization rate to be large. There could therefore be strong competition between ionization on the one hand and recombination with generation of higher harmonics on the other.

Szöke and Rhodes[43] have recently proposed that the presence of intense higher harmonics generated from a multiply excited collective excitation of the $5p$ shell in Xe might be central to the problem of $4d$ inner-shell ionization. Evidence for such inner-shell ionization has been observed at intensities around 10^{15} W cm^{-2} by Rhodes and co-workers,[11] who interpret line structures in their photoelectron spectra in terms of $4d$ Auger lines.

Figures 14(b)–14(e) provide examples of $4d$ inner-shell ionization driven by a $5p$ outer-shell multielectron resonance with generation of higher harmonics, if we put $i=4d$ and let all other hole lines be $5p$. In this case, Fig. 14(f) describes the process that both the inner and the outer shells become ionized at the same time (i.e., within the same laser pulse).

Boyer and Rhodes[19] have also proposed a mechanism for $4d$ ionization where the entire $5p$ shell is collectively accelerated by the field towards the $4d$ shell. If this collective excitation remains bound *(large amplitude oscillation),* then the diagrammatic processes in Figs. 14(c)–14(e) precisely correspond to this situation, describing energy transfer via different harmonics and multiple fields. If, on the other hand, the multiple $5p$ excitation becomes unbound *(collective 5p ionization,* as suggested by Boyer and Rhodes[19]), then Fig. 14(g) gives an example of a possible diagrammatic process, where an essential part involves $4d$ ionization via scattering by the $5p$ photoelectron current.

The final question then becomes, What is the relevance of using *linear response* for describing screening of a pulsed laser field by atomic electrons? At sufficiently high intensities, the answer obviously has to be none whatsoever. However, the problem is that the nonlinear response of a real atom is not well understood and, consequently, the conditions for breakdown of linear response

are not known. Moreover, the problem is a dynamic one, because the laser pulse has a finite rise time and duration. As long as those time scales are long compared with typical atomic (electronic) time scales, the external laser intensity will effectively rise very slowly from zero towards its peak value. Then *linear response* must necessarily be relevant during at least the *beginning of the laser pulse.*

Another important point, as recently emphasized by Lambropoulos,[39] is that much of the action takes place long before a very intense pulse has had time to reach its peak value. Lambropoulos[39] has shown that the first ionization stages of Xe (Xe^+, Xe^{2+}) are created on a time scale of 0.1 ps at intensities of 10^{13}–10^{14} W cm^{-2}, which should lead to stepwise ionization of the outermost shell. We conclude that, under these circumstances, it is difficult (impossible) to build up large-amplitude collective motion of the $5p$ shell. We therefore suggest that up to intensities of 10^{13}–10^{14} W cm^{-2}, this type of nonlinearity may be neglected. On the other hand, inner-shell $4d$ ionization, if correctly identified,[11] needs intensities approaching 10^{15} W cm^{-2}. In this case, nonlinear effects can be expected to be prominent,[43] at least if the pulse time is sufficiently short that stepwise ionization does not have time to occur until a large-amplitude motion has been excited. Possibly, there could be an intermediate situation with high harmonics induced in a partially stripped $5p$ shell.[45]

In conclusion, we suggest that linear response and linear screening of the external laser field is relevant and important for laser intensities approaching the 10^{13}–10^{14} W cm^{-2} range. We propose that it therefore must be taken into account when describing multistep ionization of atomic outer shells,[45] leading, e.g., to a reduction of the effective intensity in the $5p$ region of Xe by a factor of 2 ($\omega=0$) to 4 ($\omega=6$ eV).

We furthermore propose that in the inner-shell $4d$ region of Xe (and similar systems) the effective intensity will be so low as to make impossible direct multiphoton $4d$ ionization. We suggest that inner-shell ionization should not occur until the effective intensity increases to a point where nonlinear effects and/or outer shell stripping become important.

VI. CONCLUSION

As has been shown by recent experiments,[7–11] the interaction of a many-electron atom with a strong laser field involves complex processes, multiple excitations and ionizations. We have developed a formalism within the framework of many-body perturbation theory and diagrammatic techniques, which enables us to describe multiple multiphoton ionization of many-electron atoms. In this first paper, we have studied the influence of screening effects on one-electron multiphoton ionization.

We have calculated the one-electron multiphoton ionization current including the Stark shift to first order in the intensity and including many-electron polarization effects within the RPA. This is done by renormalizing the electron-photon coupling both in the radiation and the Coulomb fields. The key result obtained is the following: the one-electron current has the same form for an interacting-electron system as for a noninteracting-electron system, but with the external laser intensity replaced by an effective local (space-dependent) intensity. The influence of screening effects in multiphoton ionization is therefore connected to the spatial variations of the effective field which is experienced by the electrons.

The theory has been applied to calculations of one-photon and two-photon ionization cross sections of helium in the weak-field limit. The one-electron wave functions are calculated using a LDA potential. The photoionization cross section (LDRPA) calculated from 1.5 to 8 Ry is found to be in good agreement with the experimental cross section[60] and another similar calculation[59] (RPAE). The two-photon ionization cross section is calculated from 0.6 to 2.5 Ry. It shows good agreement with other results[33,34] obtained within the time-dependent Hartree-Fock theory. Many-electron polarization effects have an important influence on the two-photon ionization process. The two-photon ionization cross section is lowered at low photon energies (by a factor up to 1.4) and increased at higher energies above 1.45 Ry. Such effects could have a much more dramatic influence on multiphoton ionization of heavy atoms (Xe, U).

Finally, we have discussed in detail a number of recent experimental results. We have emphasized the role of many-electron screening effects on these results. The main ideas can be summarized as follows. (i) Direct inner-shell ionization is *extremely* reduced due to screening of the field by the outermost shell. (ii) Outer-shell ionization is reduced due to screening by the other outer electrons; the importance of this effect depends on the number of electrons in the outer shell. In particular, during the stripping of an atom (Xe) through stepwise multiple ionization, the screening is progressively reduced and this leads to enhanced yields of highly charged ions compared to the lowest charged ions. Moreover, we have discussed the limitations of our treatment of many-electron effects, i.e., in the framework of linear response, and we have given some ideas about some possible extensions: nonlinear effects, multielectron resonance effects, and collective excitation and ionization processes.

This first investigation of the influence of many-electron effects in multiphoton ionization is obviously very encouraging. More extended numerical calculations (other atoms, more electrons, more photons, etc.) would be helpful to support some ideas presented in this paper and to gain a better understanding of the problem. The study of two-electron multiphoton ionization will be developed in a forthcoming paper.

ACKNOWLEDGMENTS

One of us (A.L.) would like to thank Dr. M. Trahin for many stimulating discussions and for reading the manuscript. She would also like to thank Chalmers University of Technology for kind hospitality and financial support. This work has been supported by the Swedish Natural Science Research Foundation (NFR).

APPENDIX A

This appendix describes the numerical methods used for calculating screened one-photon and two-photon ma-

trix elements. Radial, angular, and spin variables have not been separated so far. In this appendix, we first deal with the angular integration and spin summation of the different quantities involved in the expressions for the one- and two-photon ionization probabilities. Then we present the numerical methods used to calculate the radial parts of the response function $\epsilon^{-1}(\mathbf{r},\omega)$ and the Green's function $G(\mathbf{r},\mathbf{r}',\omega)$. The last problem presented in this appendix concerns the numerical calculation of continuum-continuum dipole matrix elements.

1. Angular integration and spin summation

The coefficient due to the angular integration and spin summation involved in the photoionization cross section (Eq. 4.3) is

$$C_{\varepsilon i}=\frac{N_i}{3}(2l_\varepsilon+1)\begin{bmatrix} l_i & 1 & l_\varepsilon \\ 0 & 0 & 0 \end{bmatrix}^2 , \tag{A1}$$

where N_i is the number of electrons of shell i, l_i, and l_ε are the orbital momenta of the initial and final states, respectively. For helium, $C_{\varepsilon p\,1s}=\frac{2}{3}$.

The RPA expansion (Fig. 7) consists of an infinite series of bubble diagrams. Two successive bubbles must have hole levels with different quantum numbers.[57,58,65] Physically, this means that an electron-hole excitation cannot interact with its own field (no self-interaction). As a consequence, the coefficient involved in the RPA equation for a single channel $i\rightarrow\varepsilon$ [e.g., Eq. (3.23)] is

$$\tilde{C}_{\varepsilon i}=\frac{N_i-1}{3}(2l_\varepsilon+1)\begin{bmatrix} l_i & 1 & l_\varepsilon \\ 0 & 0 & 0 \end{bmatrix}^2 . \tag{A2}$$

For helium, $\tilde{C}_{\varepsilon p\,1s}=\frac{1}{3}$. For a single electron, $N_i=1$, there is no interaction at all.

Lastly, the coefficients involved in the two-photon ionization rate are $C_{\varepsilon l n p}C_{n p\,1s}/2$ with $l=s$ or d (0.1778 and 0.2222, respectively).

2. Radial integration

Having done these angular integrations and spin summations, we assume that the expressions below are related to radial variables. The one- and two-photon radial matrix elements can then be written as

$$d_{\varepsilon i}(\omega)=\langle \varepsilon \mid \epsilon^{-1}(r,\omega)r \mid i\rangle , \tag{A3a}$$

$$d^2_{\varepsilon i}(\omega)=\langle \varepsilon \mid \epsilon^{-1}(r,\omega)rG(r,r',\omega)\epsilon^{-1}(r',\omega)r' \mid i\rangle . \tag{A3b}$$

The response function (or inverse dielectric function) satisfies the following equation [from Eq. (3.26)]:

$$\epsilon^{-1}(r,\omega)=1-\sum_n \tilde{C}_{ni}\frac{2\omega_{ni}[Y^1_{ni}(r)/r]d_{ni}(\omega)}{\omega^2_{ni}-\omega^2} , \tag{A4}$$

where

$$Y^1_{ni}(r)=\int_0^{+\infty} u^*_n(r')u_i(r')\frac{r_<}{r^2_>}dr' , \tag{A5}$$

$r_<=\inf\{r,r'\}$, $r_>=\sup\{r,r'\}$. Equation (A4) is solved by using the Fredholm approximation (cf. Sec. III A)

$$\epsilon^{-1}(r,\omega)=1-\sum_n \tilde{C}_{ni}\frac{2\omega_{ni}[Y^1_{ni}(r)/r]d_{ni}}{\omega^2_{ni}-\omega^2}\Big/\epsilon(\omega) , \tag{A6}$$

with

$$\epsilon(\omega)=1-\sum_n \tilde{C}_{ni}\frac{2\omega_{ni}V_{inni}}{\omega^2_{ni}-\omega^2} . \tag{A7}$$

The two-photon matrix element (A3b) requires the evaluation of the Green's function $G(r,r',\omega)$ defined by

$$G(r,r',\omega)=\sum_n \frac{u^*_n(r)u_n(r')}{\omega_{ni}-\omega} , \tag{A8}$$

or equivalently, the wave packet (or "perturbed" wave function)

$$u_{\tilde{\omega}}(r)=\int G(r,r',\omega)\epsilon^{-1}(r',\omega)r'u_i(r')dr' , \tag{A9a}$$

$$u_{\tilde{\omega}}(r)=\sum_n \frac{u_n(r)d_{ni}(\omega)}{\omega_{ni}-\omega} . \tag{A9b}$$

In both cases, the summation is performed explicitly over intermediate states n which all lie in the continuum due to the local-density approximation. About 250 points are used over an energy range 0.02–20 Ry.

As soon as the photon energy ω is greater than the ionization energy, the wave packet $|\tilde{\omega}\rangle$ (A9) has the behavior of a continuum wave function and the two-photon matrix element $\langle \varepsilon \mid \epsilon^{-1}(r,\omega)r \mid \tilde{\omega}\rangle$ involves two functions oscillating to infinity. In the last part of this appendix, we describe the method used for calculating continuum-continuum matrix elements. For simplicity, we deal with unscreened matrix elements $\langle u_1 \mid r \mid u_2\rangle$.

3. Continuum-continuum matrix elements

Continuum wave functions are normalized so that (Ry units)

$$u_\varepsilon(r)=(1/\pi k)^{1/2}\sin\left[kr+\frac{Z_i}{k}\ln(2kr)-l\pi/2+\eta_l\right] , \tag{A10}$$

with $k=\varepsilon^{1/2}$, Z_i is the ionicity (for the local-density potential, $Z_i=0$) and η_l the phase shift.

The phase-amplitude development of a continuum wave function is[66]

$$u_\varepsilon(r)=(1/\pi z)^{1/2}\sin\left[\int z\,dr\right] , \tag{A11}$$

with z solution of the differential equation

$$z^2=\lambda+z^{1/2}\frac{d^2}{dr^2}z^{-1/2} , \tag{A12}$$

$$\lambda=k^2+\frac{2Z_i}{r}-\frac{l(l+1)}{r^2}+\cdots . \tag{A13}$$

Continuum-continuum matrix elements are calculated by the following method: the integration from 0 to a chosen R is performed numerically; the integral from R to infinity is then analytically approximated using the develop-

ment (A11). Let u_1, u_2 be two continuum wave functions with energies $\varepsilon_1, \varepsilon_2$. The integral from R to infinity may be written

$$\int_R^{+\infty} u_1(r) r u_2(r) dr = I_+ - I_- \tag{A14}$$

with

$$I_\pm = -\int_R^{+\infty} \frac{r}{2\pi(z_1 z_2)^{1/2}} \cos(v_\pm) dr \ , \tag{A15}$$

$$z_\pm = z_1 \pm z_2 \ , \tag{A16}$$

$$v_\pm = \int z_\pm dr \ . \tag{A17}$$

$I_\pm$ is calculated by parts,[67]

$$I_\pm = \left[\frac{xr}{2z_\pm} \sin(v_\pm) + \frac{1}{2z_\pm} \cos(v_\pm) \frac{d}{dr} \left[\frac{xr}{z_\pm} \right] + \cdots \right]_{r=R} \tag{A18}$$

with

$$x = (z_1 z_2)^{1/2} \ . \tag{A19}$$

This development usually converges with three terms. Moreover, it was found that the value of R can be chosen just outside the core region (about 10 a.u. for helium).

APPENDIX B

This appendix briefly discusses the relative importance of polarization effects represented in Fig. 10. The diagrams 10(b) which have not been calculated involve a monopole Coulomb interaction for the transition $1s \rightarrow \varepsilon s$ and a quadrupole Coulomb interaction for the transition $1s \rightarrow \varepsilon d$. The ratios of monopole, dipole, and quadrupole Coulomb interactions are 1:0.6:0.06 at a typical energy value 1 Ry [the radial Slater integrals $G^l(1s, \varepsilon l)$ are approximately constant over a wide energy range]. These ratios include the spin-summation–angular-integration coefficient equal to $2/(2l+1)$. The contribution of quadrupole interaction is negligible. The total ionization rate is mostly given by the transition $1s \rightarrow \varepsilon d$, except just at the threshold (Fig. 12) where the contribution of the transition $1s \rightarrow \varepsilon s$ is important. Consequently, the contribution of correlation effects represented in Fig. 10(b) will not much modify the ionization rate, except perhaps in the threshold region (then in reality in the two-photon absorption spectrum).

[1] P. Lambropoulos, Adv. At. Mol. Phys. **12**, 87 (1976).
[2] J. Morellec, D. Normand, and G. Petite, Adv. At. Mol. Phys. **18**, 97 (1982).
[3] G. Mainfray and C. Manus, in *Multiphoton Ionization of Atoms*, edited by S. L. Chin and P. Lambropoulos (Academic, New York, 1984), p. 7; Y. Gontier and M. Trahin, in *ibid.*, p. 35.
[4] P. Agostini, F. Fabre, and G. Petite, in *Multiphoton Ionization of Atoms*, edited by S. L. Chin and P. Lambropoulos (Academic, New York, 1984), p. 133.
[5] P. Kruit, J. Kimman, H. G. Muller, and M. Van der Wiel, Phys. Rev. A **28**, 248 (1983).
[6] L. A. Lompré, A. L'Huillier, G. Mainfray, and J. Y. Fan, J. Phys. B **17**, L817 (1984).
[7] A. L'Huillier, L. A. Lompré, G. Mainfray, and C. Manus, Phys. Rev. A **27**, 2503 (1983).
[8] A. L'Huillier, L. A. Lompré, G. Mainfray, and C. Manus, J. Phys. B **16**, 1363 (1983).
[9] K. Boyer, H. Egger, T. S. Luk, H. Pummer, and C. K. Rhodes, J. Opt. Soc. Am. B **1**, 3 (1984).
[10] T. S. Luk, U. Johann, H. Egger, H. Pummer, and C. K. Rhodes, Phys. Rev. A **32**, 214 (1985).
[11] C. K. Rhodes, Science **229**, 1345 (1985).
[12] H. G. Muller and A. Tip, Phys. Rev. A **30**, 3039 (1984).
[13] M. Edwards, L. Pan, and L. Armstrong, Jr., J. Phys. B **18**, 1927 (1985).
[14] Z. Bialynicka-Birula, J. Phys. B **17**, 3091 (1984).
[15] Z. Deng and J. H. Eberly, J. Opt. Soc. Am. **2**, 486 (1985).
[16] A. Szöke, J. Phys. B **18**, L247 (1985).
[17] S. L. Chin, F. Yergeau, and P. Lavigne, J. Phys. B **18**, L213 (1985).
[18] L. V. Keldysh, Zh. Eksp. Teor. Fiz. **47**, 1945 (1964) [Sov. Phys.—JETP **20**, 1307 (1965)].
[19] K. Boyer and C. K. Rhodes, Phys. Rev. Lett. **54**, 1490 (1985).
[20] G. Wendin, Comments At. Mol. Phys. **17**, 115 (1986).
[21] T. Åberg, A. Blomberg, J. Tulkki, and O. Goscinski, Phys. Rev. Lett. **52**, 1207 (1984).
[22] M. Crance, J. Phys. B **17**, 3503, L635 (1984); **17**, 4333 (1984); **17**, L635 (1984); **18**, L155 (1955).
[23] S. Geltman, Phys. Rev. Lett. **54**, 1909 (1985).
[24] G. Wendin, in *New Trends in Atomic Physics*, "Les Houches," Session XXXVIII, edited by G. Grynberg and R. Stora (Elsevier, New York, 1984).
[25] G. Wendin, Phys. Rev. Lett. **53**, 724 (1984).
[26] A. F. Starace, Appl. Opt. **19**, 4051 (1980).
[27] M. Ya. Amusia and N. A. Cherepkov, Case Stud. At. Phys. **5**, 47 (1975); M. Ya. Amusia, Adv. At. Mol. Phys. **17**, 1 (1981); Appl. Opt. **19**, 4042 (1980).
[28] H. P. Kelly, in *Atomic Physics 8*, edited by I. Lindgren, A. Rosén, and S. Svanberg (Plenum, New York, 1983), p. 305.
[29] A. Zangwill and P. Soven, Phys. Rev. Lett. **45**, 204 (1980); Phys. Rev. A **21**, 1561 (1980).
[30] A. Zangwill, in *Atomic Physics 8*, edited by I. Lindgren, A. Rosén, and S. Svanberg (Plenum, New York, 1983), p. 339.
[31] W. R. Johnson, C. D. Lin, K. T. Cheng, and C. M. Lee, in Proceedings of the Nobel Symposium 46, edited by I. Lindgren and S. Lundqvist [Phys. Scr. **21**, 409 (1980)].
[32] A. Zangwill, J. Chem. Phys. **78**, 5926 (1983).
[33] G. A. Victor, Proc. Phys. Soc. **91**, 825 (1967).
[34] B. Ritchie, Phys. Rev. A **16**, 2080 (1977).
[35] M. S. Pindzola and H. P. Kelly, Phys. Rev. A **11**, 1543 (1975).
[36] R. Moccia, N. K. Rahman, and A. Rizzo, J. Phys. B **16**, 2737 (1983).
[37] M. Crance, in *Fundamentals of Laser Interactions*, Vol. 229 of *Lecture Notes in Physics*, edited by F. Ehlotzky (Springer-Verlag, Berlin, 1985), p. 136.
[38] M. Crance and M. Aymar, J. Phys. (Paris) **46**, 1887 (1985).
[39] P. Lambropoulos, Phys. Rev. Lett. **55**, 2141 (1985).
[40] P. Gangopadhyay, X. Tang, P. Lambropoulos, and R. Shakeshaft, Bull. Am. Phys. Soc. **30**, 858 (1985); Phys. Rev. A (to be published).
[41] A. F. Starace and P. Zoller, in Ref. 37, p. 292.

[42]P. Froelich and A. Flores-Riveros, J. Chem. Phys. (to be published).
[43]A. Szöke and C. K. Rhodes, Phys. Rev. Lett. **56**, 720 (1986).
[44]A. Szöke (unpublished).
[45]G. Wendin, L. Jönsson, and A. L'Huillier, Phys. Rev. Lett. **56**, 1241 (1986).
[46]W. Brandt, L. Eder, and S. Lundqvist, J. Quant. Spectrosc. Radiat. Transfer **7**, 411 (1967).
[47]P. Agostini and G. Petite, J. Phys. B **17**, L811 (1984).
[48]G. Wendin, J. Phys. B **3**, 455 (1970).
[49]H. P. Kelly, Phys. Rev. **136**, B896 (1964).
[50]I. Lindgren and J. Morrison, *Atomic Many-Body Theory,* Vol. 13 of *Springer Series in Chemical Physics* (Springer-Verlag, Berlin, 1982).
[51]Y. Gontier, N. K. Rahman, and M. Trahin, Phys. Rev. A **14**, 2109 (1976).
[52]E. Arnous, J. Bastian, and A. Maquet, Phys. Rev. A **27**, 977 (1983).
[53]A. Maquet, Shih-I Chu, and W. P. Reinhardt, Phys. Rev. A **27**, 2946 (1983).
[54]In the case of N-photon ionization with $N>1$, the second term in Eq. (3.14) should represent an approximation. It describes a Stark shift due to emission followed by reabsorption [Fig. 3(e)], and the result probably includes some effects of double counting when $N>1$.
[55]Z. Crljen, Ph.D. thesis, University of Zagreb, 1984; Z. Crljen and G. Wendin (unpublished).
[56]W. Brandt and S. Lundqvist, Phys. Rev. **132**, 2135 (1963).
[57]G. Wendin, J. Phys. B **5**, 110 (1972); **6**, 42 (1973).
[58]Z. Crljen and G. Wendin, Phys. Scr. **32**, 359 (1985).
[59]G. Wendin, Phys. Lett. **33A**, 16 (1970); J. Phys. B **4**, 1080 (1971).
[60]C. V. Marr and J. B. West, At. Data Nucl. Data Tables **18**, 497 (1976).
[61]A. Dalgarno and G. A. Victor, Proc. R. Soc. London Ser. A **291**, 291 (1966).
[62]G. Wendin, in *Photoionization and Other Probes of Many-Electron Interactions,* Vol. B18 of NATO ASI, edited by F. J. Wuilleumier (Plenum, New York, 1976).
[63]G. Wendin, Struct. Bonding (Berlin) **45**, 1 (1981).
[64]L. A. Lompré, A. L'Huillier, G. Mainfray, and C. Manus, Phys. Lett. **112A**, 319 (1985).
[65]This is a physical argument. Technically, complete inclusion of all the relevant diagrams automatically provides the cancellations required by physics. The diagonal (self-interaction) bubble diagram is canceled by a self-exchange diagram contributing to the exchange potential. This is properly treated within the Hartree-Fock approach while the LDA represents an approximation. However, we think that the present approach is reasonable. In particular, it does not overestimate the effects of many-electron screening.
[66]A. L. Stewart, Adv. At. Mol. Phys. **3**, 151 (1967).
[67]M. Aymar and M. Crance, J. Phys. B **13**, L287 (1980).